**Atmospheric
Chemistry
and Physics
Discussions**

GOMOS O$_3$, NO$_2$, and NO$_3$ observations in 2002–2008

**E. Kyrölä[1], J. Tamminen[1], V. Sofieva[1], J. L. Bertaux[2], A. Hauchecorne[2],
F. Dalaudier[2], D. Fussen[3], F. Vanhellemont[3], O. Fanton d'Andon[4], G. Barrot[4],
M. Guirlet[4], T. Fehr[5], and L. Saavedra de Miguel[5]**

[1]Finnish Meteorological Institute, Earth Observation, Helsinki, Finland
[2]Laboratoire Atmosphères, Milieux, Observations Spatiales, Université Versailles St.-Quentin, CNRS-INSU, Verrières-le-Buisson, France
[3]Institut d'Aéronomie Spatiale de Belgique, Brussels, Belgium
[4]ACRI-ST, Sophia Antipolis, France
[5]European Space Research Institute (ESRIN), European Space Agency, Frascati, Italy

ACPD

10, 2169–2220, 2010

**GOMOS trace gases
2002–2008**

E. Kyrölä
(erkki.kyrola@fmi.fi)

Title Page

Abstract	Introduction
Conclusions	References
Tables	Figures

|◄ | ►|
◄ | ►

Back | Close

Full Screen / Esc

Printer-friendly Version

Interactive Discussion

Abstract

The Global Ozone Monitoring by Occultation of Stars (GOMOS) instrument onboard the European Space Agency's ENVISAT satellite measures ozone, NO_2, NO_3, H_2O, O_2, and aerosols using the stellar occultation method. Global coverage, good vertical resolution and the self-calibrating measurement method make GOMOS observations a promising data set for building various climatologies and time series. In this paper we present GOMOS nighttime measurements of ozone, NO_2, and NO_3 during six years 2002–2008. Using zonal averages we show the time evolution of the vertical profiles as a function of latitude. In order to get continuous coverage in time we restrict the latitudinal region to 50° S–50° N. Time development is analysed by fitting constant, annual and semi-annual terms as well as solar and QBO proxies to the daily time series. Ozone data cover the stratosphere, mesosphere and lower thermosphere (MLT). NO_2 and NO_3 data cover the stratosphere. In addition to detailed analysis of profiles we derive total column distributions using the fitted time series.

The time-independent constant term is determined with a good accuracy (better than 1%) for all the three gases. The median retrieval accuracy for the annual and semi-annual term varies in the range 5–20%. For ozone the annual terms dominate in the stratosphere giving early winter ozone at mid-latitudes. Above the ozone layer the annual terms change the phase which results to ozone summer maximum up to 80 km. In the MLT the annual terms dominate up to 80 km where the semiannual terms start to grow. In the equatorial MLT the semi-annual terms dominate the temporal evolution whereas in the mid-latitude MLT annual and semi-annual terms compete evenly. In the equatorial stratosphere the QBO dominates the time development but the solar term is too weak to be determined. In the MLT above 85 km the solar term grows significant and ozone has 15–20% dependence on the solar cycle. For NO_2 below the maximum at 30 km the annual summer maxima dominates at mid-latitudes whereas in the equatorial region a strong QBO prevails. For NO_3 the annual variation dominates giving rise to summer maxima. The NO_3 distribution is controlled by temperature.

1 Introduction

GOMOS (Global Ozone Monitoring by Occultation of Stars) is a stellar occultation instrument onboard the ENVISAT satellite (see Bertaux et al. (1991, 2000, 2004); Kyrölä et al. (2004); ESA (2001), http://envisat.esa.int/dataproducts/gomos and other articles of this special volume). GOMOS measurements start at altitude of 130 km and the first few measurements are used to determine star's undisturbed spectrum (the reference spectrum). The horizontal transmission spectra are calculated from the star spectra measured through the atmosphere and the reference spectrum. The integration time is 0.5 s, which gives the altitude sampling resolution of 0.5–1.6 km depending on the tangent altitude and the azimuth angle of the measurement. GOMOS measures during day and night but only nighttime measurements have been validated so far.

The spectral ranges of GOMOS detectors are 248–690 nm, 755–774 nm, and 926–954 nm, which make it possible to retrieve vertical profiles of O_3, NO_2, NO_3, H_2O, O_2, and aerosols. In this work we are concentrating on the three first mentioned constituents and they are retrieved from the UV-visible spectral range. The retrieved ozone profiles have 2 km vertical resolution below 30 km and 3 km above 40 km. NO_2 and NO_3 have 3 km vertical resolution at all altitudes. The details of the retrieval algorithms are discussed in Kyrölä et al. (2004); ESA (2001), http://envisat.esa.int/dataproducts/gomos and in other articles of this special volume.

GOMOS measurements provide a possibility to investigate nighttime global vertical distributions of ozone, NO_2, and NO_3 distributions from the tropopause up to the mesosphere and even to the lower thermosphere (ozone only). We have earlier presented ozone distributions for the year 2003 in Kyrölä et al. (2006) and NO_2, and NO_3 distributions in Hauchecorne et al. (2005). Now we can extend the analysis over the six year period 2002–2008. The longer period makes it possible to study various natural cycles in data. We will retrieve annual and semi-annual variation as well as variation due to the solar cycle and the quasi-biennial oscillation (QBO). The period consider is, however, too short to study anthropogenic trends in data. Besides providing new insights

to the atmospheric dynamics and chemistry, the analysis gives valuable information about the GOMOS product quality and the consistency of the data sets.

In Sect. 2 we present the selection of data used for analysis. The method used in the time series fitting is detailed in Sect. 3. Sections 4–6 show results for ozone, NO_2 and NO_3, respectively. For each gas we present first time evolution of profiles using monthly and 20-degree latitudinal averages. The times series fitting is based on daily data and 10-degree latitudinal averages. We show the time-averaged constant term and various cyclic components of the vertical profiles. We also calculate vertical column densities using the time series fits of profiles.

2 Selection of data

Like for all new instruments, a lot of effort has been targeted to GOMOS geophysical validation and comparisons with results from other instruments. GOMOS data validation activity has been carried out since the summer of 2002. A comprehensive validation of ozone profiles against ground-based and balloon-borne instruments has been presented in Meijer et al. (2004). Results show that in dark limb GOMOS ozone profile data agree very well with the correlative data: between 14 and 64 km altitude their differences show only a small (2.5–7.5%) negative bias with a standard deviation of 11–16% (19–63 km). From comparisons with other satellite instrument we can mention, for example, the extensive ACE validation study in Dupuy et al. (2009) and the GOMOS-MIPAS comparison including also mesospheric altitudes in Verronen et al. (2005). GOMOS NO_2 measurements have been compared with HALOE results in Hauchecorne et al. (2005), with MIPAS results in Verronen et al. (2009) and with ACE-FTS results in Kerzenmacher et al. (2008). For NO_3 we have validation with balloon borne instrument in Renard et al. (2008). A review of aforementioned studies and other GOMOS validation studies are presented elsewhere in this special volume.

In this work we use GOMOS dark limb measurements only by requiring the solar zenith angle at the tangent point to be greater than 107°. In Fig. 1 we have shown

the distribution of GOMOS night-time measurements during 2002–2008. The good coverage of the winter poles and the missing coverage of the summer poles are evident. During May–June 2003 and December–August 2005 GOMOS suffered from a malfunctioning of the pointing system. In 2003 this can be seen only as a moderate decrease in the number of measurements but in 2005 a real gap in the measurements is evident. New pointing system related problems appeared during 2009 but this study is restricted to 2002–2008. The instrumental problems of GOMOS have forced to restrict the azimuth range of the pointing system from the original −10° to 90° to a window of 20° with a variable center. These changes mean that the selection of stars has not been constant during the time frame of this study.

The solar zenith angle limit 107° together with the ability of GOMOS to follow and measure stars outside the orbital plane of ENVISAT leads to a variation in the local hour of measurements. This is important for measurements of diurnally varying constituents NO_2, NO_3 and ozone in the MLT. ENVISAT crossing times of the equator are 10:00 and 22:00 local time. GOMOS tangent point local times cover 1.5 h in the equator and 3 h at mid-latitudes as shown in Fig. 2.

To assure the reliability of GOMOS data during the whole time period considered, we have paid special attention to the quality of retrievals from each star individually. In Kyrölä et al. (2006) we studied the quality of GOMOS measurements during 2003 and found that stars with magnitude weaker than 1.9 (i.e. magnitude larger than) and cooler than 7000 K may easily fail to capture the whole ozone profile 15–100 km. During the course of time GOMOS S/N-ratios have decreased due to aging of the instrument. We have examined data quality for the 6 year period and compared, for example, time series formed by individual stars. In order to guarantee data quality and consistency over the whole time period considered we have removed all ozone measurements from 57 different stars. The temperatures and magnitudes of these stars fulfil approximately the limits mentioned above. For NO_2, and NO_3 all stars were used without regard of magnitude or temperature of the stars. In all data sets we rejected occultations with obliquity angle larger than 80°. The total number of dark limb occultations 2002–2008

were then 277 449 for NO_2 and NO_3 and 173 223 for ozone.

In the climatological plots and in the time series analysis we have adopted the following data gridding:

– Vertical: data is linearly interpolated to a uniform 1 km grid 15–100 km. Flagged
5   data points are not used in the analysis. Ozone profiles from 57 cool and dim
stars were not used in statistical calculations.

– Zonal: we have ignored zonal variations.

– Latitudinal: in climatological figures we have used 20° latitudinal bands. In time
series analysis we have used 10-degree latitude bands with the exception of the
10   equatorial belt 10° S–10° N. Time series analysis is done for the region 50° S–
50° N where no seasonal data voids exist.

– Time: in the climatological analysis we have used monthly time step. In time
series analysis daily step is used.

As a statistical average we have used median values as the median is more robust
15 against outliers than the normal mean estimator. The error of the median value is
taken as the interquartile range multiplied by $\frac{3}{2}$ divided by the square root of the number of cases. In order to take into account the inefficiency of the median estimator we
multiply this further by 1.7. The minimum number of measurements needed for statistical estimation has been set to 5. For smaller number of measurements we have
20 ignored the contribution. Typical median number of measurements in the equatorial
20-degree latitude belt is 280 in a month. In a day the corresponding median is 14.

The GOMOS data used for this analysis are produced by the ESA Level 2 operational
processor version 5. This version deviates only slightly from the earlier processor
version 4. The upcoming version 6 improves the level 1 calibration and implements
25 the so-called full covariance matrix in the spectral inversion. The calibration update
may somewhat alleviate the problem with weak and cool stars and then increase the
number of useful occultations. The full covariance matrix will make the GOMOS error

estimates more realistic. In this work we are not using error estimates in analysis except in the calculation of variabilities. We expect, therefore, that the results obtained in this work can be compared to earlier results and that they remain relevant for future studies using the upcoming processor version.

3 Methods

The time series analysis is based on the fitting the daily median profiles in each latitude belt with the following model:

$$
\rho^{\text{fit}}(z,t) =
$$
$$
c(z) + s(z)F_{10.7}(t) + q_1(z)F^{10}_{qbo}(t) + q_2(z)F^{30}_{qbo}(t)
$$
$$
+ \sum_{n=1}^{2}(a_n(z)\cos(nwt) + b_n(z)\sin(nwt)) \tag{1}
$$

where $w = 2\pi/365.25$ This series includes three geophysical proxies. $F_{10.7}$, the solar 10.7 cm radio flux, is a proxy for solar influence on the middle atmosphere. F^{10}_{qbo} and F^{30}_{qbo} are the equatorial winds at 10 hPa and at 30 hPa, respectively. They are proxies for quasi-biennial effects (QBO). The observational basis for these proxies are discussed in Harris et al. (1999) and WMO (2007) and references therein.

We have normalised the solar and QBO terms in Eq. (1) as

$$
f(t) = 2(f(t) - \langle f(t) \rangle)/(f_{\max} - f_{\min}) \tag{2}
$$

where <> represents average over the six year period considered. Normalised proxies are shown in Fig. 3. Note that for the solar term many authors have adopted a convention where changes are measured in one hundred F10.7 units. F10.7 values have decreased from about 180 units in 2002 to 67 units in 2008 i.e., the change is 113 units. Note also that the declining phase of the solar cycle during our data period

has been quite unusual in length. A time delay in a QBO proxy is often introduced for non-equatorial regions. Using two QBO terms, that are almost in quadrature in time (see Fig. 3), makes the time delay unnecessary.

The purpose of the normalisation in Eq. (2) is to make all the coefficients directly comparable with each other. Moreover, by selecting the time period to be exactly whole number of years (6 years 1 September 2002–31 August 2008) the time average of the series ρ^{fit} equals to the constant term. Notice that this average differs from the time average of the measured GOMOS data because of gaps in data whereas the time series in Eq. (1) is defined for all the days.

A linear trend term is manifestly missing from the time series Eq. (1). Looking at the solar proxy in Fig. 3 we can see that in the time period considered, the time smoothed solar proxy deviates from a linear trend only slightly. The linear and solar term are, therefore, highly similar. We have selected the solar term over the linear term as the former has more structure in time and therefore stronger "fingerprint".

In the case of stratospheric ozone the annual term in Eq. (1) can be justified because of the annual variation of the Brewer-Dobson meridional circulation and the annual variation of the solar insolation. In the mesosphere the meridional pole-to-pole circulation changes the direction semi-annually and this is one justification for the semi-annual term in Eq. (1). Adding higher harmonic terms does not significantly improve the quality of fits.

Instead of the harmonic terms we could have used physically more direct proxies. For example, the strength of the Brewer-Dobson circulation has been explained by the estimates of the Eliassen-Palm flux at 100 hPa in Dhomse et al. (2006). We tested this possibility but no additional benefit in fitting was obtained. In order to keep the same functional model for all altitudes and constituents we have applied formula Eq. (1) everywhere.

Retrieving the time series coefficients is done by using the weighted least squares fitting. The weights are the estimated data errors for each day. In our analysis we exploit the number densities (at geometrical altitudes) because they are the natural

units for densities retrieved from GOMOS measurements. We have also experimented with fitting mixing ratio data but no clear improvements in the fit quality were evident.

The quality of the fitting has first been checked visually. More quantitative measures used are the error estimates from fitting. We have checked the autocorrelation functions for the fitting residuals and found them reasonably close to normal. We have also studied χ^2 values and the coefficient of determination R^2. The last mentioned quantity has turned out to be the most useful measure. The significance of the time series components have been investigated by fitting various component configurations and inspecting the changes in the R^2 values. As a final check for results we have done fitting using also monthly time series. Monthly and daily fits give generally fitting components that are very close to each other. Monthly R^2 values give usually larger differences for the inclusion of minor terms than the daily R^2 values.

4 Ozone

In Fig. 4 we show the time development of the ozone number density in the stratosphere based on monthly medians and 20-degree latitude belts. The evident variation in time is a seasonal cycle at mid-latitudes. During winter and spring the ozone layer moves downwards and quite a sharp peak protrudes towards the tropopause in early winter at the northern mid-latitudes. At the same time ozone densities in the layer increase. At southern mid-latitudes these changes are somewhat smoother. These changes are consequences of the large scale Brewer-Dobson circulation of ozone from the equatorial region to high-latitudes. During summer the ozone layer moves back. The equatorial ozone layer remains relatively stable in time.

Figure 5 shows the time development of ozone in the MLT. Clear semi-annual variations of the second ozone maximum appear at all latitudes. The strongest variation and highest values are seen in the equatorial distribution with maxima around the equinox times. At higher latitudes the semi-annual peaks seem to be slightly merging through the winter season. The spring peak seems to form at somewhat higher altitude than

Full Screen / Esc

Printer-friendly Version

Interactive Discussion

the fall peak. During the six years of observations the second maximum seems to be weakening.

The overall latitudinal distribution of ozone at 20 km and at 90 km are shown in Fig. 6. The 20 km surface dissects the ozone layer at mid-latitudes and shows the winter-spring ozone maxima but lies below the ozone layer at the equator. The 90 km surface is inside the second ozone layer at all latitudes. During the equinox times ozone has distributed at all latitudes, other times ozone is concentrated more above the winter pole.

In Fig. 7 we have shown the relative variability of ozone i.e. the standard deviation of ozone time series as a function of time and altitude and in three latitude belts. We have subtracted the variability of the estimated retrieval errors of GOMOS data. Below 20 km the variability is high but otherwise the overall variability in the stratosphere is low. The median over latitudes and times in the stratosphere is 5.5% (the same average for retrieval errors is 0.6%). Somewhat higher variability appears at mid-latitudes during the winter times. In the MLT a very high variability can be seen around the ozone minimum 75–85 km and reduced variability around the ozone maximum at 90 km. The median over latitudes and times in the MLT is 19% (the same average for retrieval errors is 1%).

What part of the variability is connected with the diurnal variation? In Fig. 8 we have shown the diurnal variation of ozone at three altitudes and at two latitudes as estimated from the NCAR ROSE model (see also SABER results in Huang et al. (2008)). In the lower and middle stratosphere the diurnal variations can safely be ignored. At 50 km small variation exist but it takes place outside the local time coverage of GOMOS measurements (see Fig. 2). At 70 km and 90 km strong variations can be detected but during GOMOS observing hours only the 90 km variation is significant. At the second ozone maximum the variation is ±8% but only at the equator.

In order to get a more quantitative view into the systematic variations of the ozone distribution in time, we have carried out a time series analysis of the ozone number density profiles in the latitude range 50° S–50° N. The latitudinal limits are such that

there are no seasonal gaps in data (as would be in polar areas). Figure 9 shows an example of the time series fitting to the ozone number density data at 90 km in the latitudinal belt 40° N–50° N. The figure also includes the corresponding fit residual and the individual fitting components. The solar, QBO and harmonic terms are in relative units with respect to the constant term (not shown in this figure). Figure 9 shows that the fit at 90 km is able to follow reasonably well the large semi-annual oscillation of ozone and it also shows a declining mean ozone content from the solar term in the MLT. The fit fails to replicate the high ozone values seen above the sinusoidal maxima (for high values of ozone in the MLT, see Smith et al., 2008).

The constant term profiles at different latitudes are shown in Fig. 10. The constant term has a low median fitting error of 0.16%. The profiles show the stratospheric main ozone layer and the secondary ozone layer in the MLT. Besides the two maxima, the deep ozone minimum around 80 km is noteworthy. The stratospheric and MLT contributions are nearly symmetric with respect to the equator. The main peak altitude is latitude dependent whereas the MLT structure (minimum and the second maximum) is almost independent of latitude. If we calculate the total ozone from the constant term in the range 15–100 km the ozone column is 244 Dobsons in the equator, 264 Dobsons in south mid-latitudes and 271 Dobsons in north mid-latitudes.

The annual, semi-annual, QBO and solar amplitudes for the stratosphere are shown in Fig. 11 and for the MLT in Fig. 12. The relative errors of the harmonic components vary considerably as a function of altitude. The median (over latitudes 50° S–50° N and altitudes 20–100 km) error values are in the range 5–15%. The annual amplitudes (a_1 and b_1) dominate over the semi-annual ones (a_2 and b_2). Below 25 km the annual amplitude increases (absolute value) at all latitudes towards the tropopause. At the equator the increase takes place below the ozone layer but at mid-latitudes it is inside the ozone layer. The two components (a_1 and b_1) have the same sign and this leads to the winter maxima of ozone in both hemispheres. The amplitude is larger at northern than at southern latitudes. The second increase of the annual amplitude a_1 takes place at mid-latitudes in 30–35 km giving rise a summer maximum. Between the lower and

Title Page

Abstract | Introduction

Conclusions | References

Tables | Figures

◄◄ | ►►

◄ | ►

Back | Close

Full Screen / Esc

Printer-friendly Version

Interactive Discussion

mid-stratosphere maxima there is an interesting deep minimum at mid-latitudes in the annual oscillation around 25 km.

In the MLT below 70 km the first (a_1) annual term dominates at mid-latitudes all other amplitudes being small. The annual amplitude (absolute value) reaches 75% in south and 50% in north at 75 km. Notice that these amplitudes have opposite signs when compared to the annual amplitudes in the ozone layer below 25 km. They lead to summer maxima. The signs are changed again when the mid-latitude annual terms go through zero at 80 km and reaches new maxima of 85% (south) and 60% (north) around 83 km. The semi-annual amplitudes start to increase after 75 km at all latitudes. In the equator the first semi-annual component (a_2) rapidly increases up to 85% at 82 km and then slowly decreases at higher altitudes. At 90 km it is 50% and dominates over other amplitudes. This gives maximum ozone density in the beginning of April and October. At mid-latitudes around the second maximum the annual and semi-annual amplitudes have nearly the same (absolute) value. The density shows a mix of annual and semi-annual cycles. An example was shown in Fig. 9.

The minor components of the time series are the solar and QBO terms. We have studied changes in the R^2-values for the fitting time series Eq. (1) where solar, QBO or both are eliminated. In the equatorial area up to 40 km the two QBO terms improve considerably the quality of the fitting. The solar term improves the fits only in the MLT above 85 km (equator and north) and above 90 km (south). Everywhere else the solar and QBO contributions to the fits are small.

In the equatorial stratosphere QBO terms have relatively large values of 8–9% between 20 and 40 km with the median relative error of 3.5%. The QBO shows two cell structure with maxima around 25 km and 38 km. In the MLT the solar term grows with altitude reaching 20–25% at 100 km with the median relative error of 8–10% above 85 km. At the second ozone maximum the solar contribution is almost zero in the SH but 17–19% at the equator and northern mid-latitudes.

The fit for the ozone times series is defined for all times during the 6 years, for all latitudes 50° S–50° N and for all altitudes 15–100 km. Therefore it is possible to

calculate various vertical column distributions. Fig. 13 shows the ozone columns in 15–100 km and in 80–100 km. The "total" column shows clearly the mid-latitude ozone winter-spring maxima and low ozone values in the equator. The lowest values in this altitude limited column distribution are seen around 15° N during winter. In the MLT the semi-annual variation prevails everywhere with largest columns at the equator. The overall structure replicates the zigzag pattern already seen in Fig. 6. The equatorial ozone shows a weakening trend.

The results obtained above can be compared with the results in literature. The limitation of the present data set to the declining part of the very peculiar solar cycle 23 must be remembered when results are compared with time series covering several solar cycles. Results about the annual and semi-annual cycles are hard to find as the time series are usually deseasonalized before the regression analysis. In Perliski et al. (1989) the authors show annual and semi-annual amplitudes in the stratosphere based on SBUV 1978–1987 measurements and a two-dimensional photochemical model. The corresponding amplitudes (of mixing ratios) from GOMOS and SBUV are quite similar.

The physical and chemical processes behind the stratospheric variations of ozone are discussed in detail in Perliski et al. (1989) and in Ko et al. (1989) and summarised in Brasseur and Solomon (2005) and in Dessler (2000). The explanation for the strong semiannual signal in the MLT has been sought from the semi-annual change of the pole-to-pole meridional circulation and from the semi-annual variation of the diurnal tide (see Smith (2004) and references therein). The former affects the H_2O amount and therefore the catalytic reactions of hydrogen with ozone. The solar tide affects O-related ozone chemistry (production and loss) and temperature. In the stratosphere and MLT the chemical modelling predicts anticorrelation of temperature and ozone.

The correlation of GOMOS monthly ozone and monthly temperature (from ECMWF) in the stratosphere is shown in Fig. 14 for four seasons and three latitude regions. In the equatorial region the correlation is for all seasons positive below 30 km and changes then to negative. This change can be understood as the transition from the region of dynamical control to the region of chemical control (see Brasseur and Solomon, 2005).

Mid-latitude correlations show similar transitions but not in so uniform way.

There are many studies on solar cycle effects on stratospheric ozone profiles. Reviews of the results can be found in Harris et al. (1999) and in WMO (2007). In our quite short data set it was not possible to extract the solar response in the stratosphere. Using longer satellite data series the solar effect has been successfully retrieved in Randel and Wu (2007); Soukharev and Hood (2006); Jones et al. (2009). In the MLT the solar cycle has been estimated only by various model simulations. In Marsh et al. (2007) the WACCM3 simulations indicate 50% increase in the ozone mixing ratio from the solar minimum to the solar maximum. In our case the changes in number densities at the second maximum are at most 20%.

Many studies have dealt with QBO effects in stratospheric ozone profiles. Reviews of the results can be found in Harris et al. (1999) and in WMO (2007). GOMOS results agree about the two cell structure in the equatorial stratosphere discussed, for example, in Randel and Wu (2007).

5 NO$_2$

The nighttime distribution of NO$_2$ from GOMOS measurements is shown in Fig. 15. A clear annual cycle is visible at mid-latitudes. The "NO$_2$ layer" around 30 km starts to expand in early winter mainly towards the tropopause but also in a lesser amount to higher altitudes. The maximum extent is reached during midsummer. After the maximum the layer contracts from the lower side while the upper boundary still increases. The minimum of the layer is reached in late fall. In the equatorial band a weak semi-annual cycle prevails. The variability of the NO$_2$ distribution (not shown) is around 20% at the maximum 30 km. The median over latitudes and times in the stratosphere is 25% (the same average for retrieval errors is 13%). The diurnal variation of NO$_2$ and NO$_3$ from the NCAR ROSE model is shown in Fig. 16. For NO$_2$ the maximum variation for the times sampled by GOMOS is at most ±6% and this takes place at the equator.

In Fig. 17 we show an example of the time series fitting in the 40° N–50° N latitude

GOMOS trace gases 2002–2008

E. Kyrölä
(erkki.kyrola@fmi.fi)

band at 30 km. In this case GOMOS data are reasonably well fitted with the annual term dominating.

The constant term in Figs. 18 and 19 shows a robust distribution around 30 km. The median fitting error is 0.4%. The maximum values are reached at mid-latitudes.
The overall distribution is quite symmetric with the equator. The partial column 20–50 km from the constant term peaks at mid-latitudes with 5.3×10^{15} cm^{-2} in south and 5.2×10^{15} cm^{-2} in north. The equator column is 3.9×10^{15} cm^{-2}.

The fitting components are shown in Fig. 20. At mid-latitudes the annual amplitude (a_1) is around 10–15% at the maximum (30 km) and grows to 60–80% below the maximum. The annual variation has been analysed from the chemistry and dynamics viewpoints in Bracher et al. (2005) and Brohede et al. (2007). At the equator the largest harmonic is semi-annual term (a_2) with the amplitude of 6%. The median error of the harmonics varies 4–12%.

Both the solar and QBO term improve the quality of the NO$_2$ fits. The median errors for solar and QBO are in the range of 14–21%. The QBO has a similar nodal structure at the equator as ozone had. The maximum amplitude of the QBO is 18% at the equator around the NO$_2$ maximum. A second, smaller peak can be found at 43 km. At mid-latitudes the QBO impact is small. The solar term at the equator shows in 25–40 km 10% negative values (i.e. more NO$_2$ during the solar minimum). At southern and northern latitudes negative values are also seen below 35 km. In south and at the equator the solar term is small in the upper stratosphere but at the northern latitudes the solar term grows to 20% at the maximum and grows positive in the upper stratosphere at northern latitudes. In Hood and Soukharev (2006) authors analyse NO$_x$ content at altitudes 32–53 km using HALOE results in 1991–2003. They found in the equatorial region negative values of 10% around 35 km and 20% around 50 km. GOMOS results agree with the first finding but do not show the large solar impact in the upper equatorial stratosphere.

Figure 21 shows the NO$_2$ total column in 20–50 km. Clear annual summer maxima at mid-latitudes and minimum values in the equatorial region. The maximum regions

seem to be slightly inclined on the time-latitude plane with the maximum delayed towards higher latitudes.

6 NO_3

The number density distribution of GOMOS NO_3 measurements is shown in Fig. 22. The "NO_3 layer" shows a remarkable extent in vertical with the maximum at 40 km. At the mid-latitudes a clear annual cycle is evident with clear asymmetry between southern and northern latitudes. The maxima seem to appear at the same time through the layer. The equatorial NO_3 shows a semi-annual cycle with maxima at the equinox times. The maxima have more variation than the ones at mid-latitudes. The variability of the NO_3 distribution (not shown) is around 30% at 40 km. The median variability over latitudes and times in the stratosphere is 56% (the same average for retrieval errors is 36%). The diurnal variability shown in Fig. 16 is about 3.5%.

Figure 23 shows a fitting example at 40 km (the number density maximum) at the southern mid-latitudes 40° S–50° S. The variation at these latitudes can be explained to a large part by the annual term. The solar and QBO terms are very small.

The latitude distribution and profiles of the constant term are shown in Fig. 24 and Fig. 25. The median fitting error is 0.6%. The constant term shows a remarkable anvil shape with a large latitudinal extent at the maximum density region around 40 km and a deep vertical extent around the equator. The distribution is nearly symmetric with respect to the equator. The total column from the constant term 25–50 km peaks in the equator with the column 34×10^{12} cm^{-2}. At southern mid-latitudes the column is 26×10^{12} cm^{-2} iand at northern mid-latitudes 25×10^{12} cm^{-2}.

The other time series coefficients are shown in Fig. 26. The annual term (a_1) dominates strongly the time evolution outside the equatorial region with the maximum amplitude of 60% in south and 40% in north. In the equatorial region the semi-annual amplitude is around 15% dominating the variation. The median errors of the harmonic components are 6–20%. The inclusion of the QBO improves the fit only in the equa-

torial region and has at the NO_3 maximum 10% amplitude. The solar term does not make difference in the fit even if the contributions in Fig. 26 are large. The median estimated error for the solar term is 30% and for the QBO 27–54%.

Figure 27 shows the total NO_3 column in 25–50 km. The total column shows clear semi-annual variation in the equatorial region and annual summer maxima with strongest maxima at the southern latitudes.

As pointed in Hauchecorne et al. (2005), the NO_3 density is controlled by a temperature sensitive reaction $NO_2+O_3 \rightarrow NO_3+O_2$. The correlation between temperature and NO_3 is shown in Fig. 28 The correlation in 30–45 km is high except the at mid-latitudes during winter when very little NO_3 can be found.

During nighttime ozone and NO_3 are nearly equilibrium and their ratio can be approximated by (Brasseur and Solomon, 2005)

$$\frac{\rho_{NO_3}}{\rho_{O_3}} = \frac{b_9}{\rho b_{12}} \tag{3}$$

where the coefficients depend on temperature. We have calculated this ratio using GOMOS monthly data for the same latitude belts used in Figs. 4 and 22. Taking the median over times the experimental and theoretical value are inside 20% from each other below 40 km for all latitude regions but deviate strongly at higher altitudes.

7 Conclusions

In this paper we have analysed 6 years of GOMOS measurements of O_3, NO_2, and NO_3. We have constructed monthly zonal climatologies and daily (and monthly) time series for the vertical profiles using GOMOS nighttime measurements. The daily time series were first examined for consistency of measurements from different stars. For ozone we found 57 stars that were not able to provide consistent ozone profile data in 15–100 km for the whole 6 year period. For NO_2 and NO_3 all stars were found useful in the 20–50 km height range. The latitudinal area analysed was restricted to 50° S–50° N

to get continuous time coverage. The polar regions were not investigated as night (or day) measurements alone cannot provide continuous coverage. GOMOS studies relevant to polar measurements of O_3, NO_2, and NO_3 are for, example, Tétard et al. (2009), Verronen et al. (2006), Seppälä et al. (2007) and Sofieva et al. (2009).

5   We analysed the time series of O_3, NO_2, and NO_3 profiles by fitting the series by a time independent constant term, annual and semi-annual terms, a solar proxy and two QBO proxies. The fitting was based on median daily values in latitude belts. The fit was also performed using monthly values and the results were found to be very close to daily results. The importance of the various terms was examined by calculating R^2
10   and χ^2 values for fits. For all three constituents the constant term, annual and semi-annual term were easily determined. For ozone the QBO terms were found important in the equatorial stratosphere. Because of the shortness of the period considered, the fitting of the solar term did not make difference in the stratospheric ozone time series but in the MLT we found large declining trends from the solar contribution. For NO_2
15   both the QBO and the solar term improved the fits at all latitudes. For NO_3 only the QBO improved the fit. The NO_3 distribution below 40 km is controlled by temperature.

The results have been shown without resorting to dynamic and chemical modelling. It is obvious that modelling is needed to understand in detail the dynamic and chemical processes behind the results. The length of data set used is still too short for a defini-
20   tive retrieval of solar cycle effects, possible CFC-related ozone recovery and climate change effects.

The GOMOS data set presented here can provide new valuable nighttime climatologies for O_3, NO_2, and NO_3 profiles. Preliminary yearly climatological data sets can be found at http://fmilimb.fmi.fi/. For stratospheric ozone there are already several clima-
25   tologies like Fortuin and Kelder (1998); Brunner et al. (2006); Randel and Wu (2007); McPeters et al. (2007); Hassler et al. (2008). In Kyrölä et al. (2006) we have made comparison of GOMOS 2003 results with the Fortuin-Kelder results but the comparison of the present 6 year GOMOS data set with the aforementioned climatologies requires a new study. The GOMOS MLT ozone data climatology is unique but a similar data

Printer-friendly Version

Interactive Discussion

set can be constructed from SABER measurements. Comparisons of MLT data with models will be very interesting as many processes in the MLT are still much more uncertain than the ones in the stratosphere. For NO_2 there exist recent climatology of Brohede et al. (2007, 2008). The NO_3 GOMOS data set is unique as most of the other instruments need sunlight to work and there is very little NO_3 during daytime.

References

Bertaux, J. L., Megie, G., Widemann, T., Chassefiere, E., Pellinen, R., Kyrölä, E., Korpela, S., and Simon, P.: Monitoring of Ozone Trend by Stellar Occultations: The GOMOS Instrument, Adv. Space Res., 11, 237–242, 1991. 2171

Bertaux, J. L., Kyrölä, E., and Wehr, T.: Stellar Occultation Technique for Atmospheric Ozone Monitoring: GOMOS on Envisat, Earth Observ. Quart., 67, 17–20, 2000. 2171

Bertaux, J. L., Hauchecorne, A., Dalaudier, F., Cot, C., Kyrölä, E., Fussen, D., Tamminen, J., Leppelmeier, G. W., Sofieva, V., Hassinen, S., d'Andon, O. F., Barrot, G., Mangin, A., Théodore, B., Guirlet, M., Korablev, O., Snoeij, P., Koopman, R., and Fraisse, R.: First results on GOMOS/Envisat, Adv. Space Res., 33, 1029–1035, 2004. 2171

Bracher, A., Sinnhuber, M., Rozanov, A., and Burrows, J. P.: Using a photochemical model for the validation of NO_2 satellite measurements at different solar zenith angles, Atmos. Chem. Phys., 5, 393–408, 2005, http://www.atmos-chem-phys.net/5/393/2005/. 2183

Brasseur, G. P. and Solomon, S.: Aeronomy of the Middle Atmosphere, Springer, Dordrecht, 3rd revised and enlarged edn., 2005. 2181, 2185

Brohede, S., McLinden, C. A., Berthet, G., Haley, C. S., Murtagh, D., and Sioris, C. E.: A stratospheric NO_2 climatology from Odin/OSIRIS limb-scatter measurements, Can. J. Phys., 85, 1253–1274, doi:10.1139/P07-141, 2007. 2183, 2187

Brohede, S., McLinden, C. A., Urban, J., Haley, C. S., Jonsson, A. I., and Murtagh, D.: Odin stratospheric proxy NOy measurements and climatology, Atmos. Chem. Phys., 8, 5731–

5754, 2008,
http://www.atmos-chem-phys.net/8/5731/2008/. 2187

Brunner, D., Staehelin, J., Maeder, J. A., Wohltmann, I., and Bodeker, G. E.: Variability and trends in total and vertically resolved stratospheric ozone based on the CATO ozone data set, Atmos. Chem. Phys., 6, 4985–5008, 2006,
http://www.atmos-chem-phys.net/6/4985/2006/. 2186

Dessler, A.: The chemistry and physics of stratospheric ozone, Academic Press, 2000. 2181

Dhomse, S., Weber, M., Wohltmann, I., Rex, M., and Burrows, J. P.: Dhomse, S., Weber, M., Wohltmann, I., Rex, M., and Burrows, J. P.: On the possible causes of recent increases in northern hemispheric total ozone from a statistical analysis of satellite data from 1979 to 2003, Atmos. Chem. Phys., 6, 1165–1180, 2006,
http://www.atmos-chem-phys.net/6/1165/2006/. 2176

Dupuy, E., Walker, K. A., Kar, J., Boone, C. D., McElroy, C. T., Bernath, P. F., Drummond, J. R., Skelton, R., McLeod, S. D., Hughes, R. C., Nowlan, C. R., Dufour, D. G., Zou, J., Nichitiu, F., Strong, K., Baron, P., Bevilacqua, R. M., Blumenstock, T., Bodeker, G. E., Borsdorff, T., Bourassa, A. E., Bovensmann, H., Boyd, I. S., Bracher, A., Brogniez, C., Burrows, J. P., Catoire, V., Ceccherini, S., Chabrillat, S., Christensen, T., Coffey, M. T., Cortesi, U., Davies, J., De Clercq, C., Degenstein, D. A., De Mazière, M., Demoulin, P., Dodion, J., Firanski, B., Fischer, H., Forbes, G., Froidevaux, L., Fussen, D., Gerard, P., Godin-Beekmann, S., Goutail, F., Granville, J., Griffith, D., Haley, C. S., Hannigan, J. W., Höpfner, M., Jin, J. J., Jones, A., Jones, N. B., Jucks, K., Kagawa, A., Kasai, Y., Kerzenmacher, T. E., Kleinböhl, A., Klekociuk, A. R., Kramer, I., Küllmann, H., Kuttippurath, J., Kyrölä, E., Lambert, J.-C., Livesey, N. J., Llewellyn, E. J., Lloyd, N. D., Mahieu, E., Manney, G. L., Marshall, B. T., McConnell, J. C., McCormick, M. P., McDermid, I. S., McHugh, M., McLinden, C. A., Mellqvist, J., Mizutani, K., Murayama, Y., Murtagh, D. P., Oelhaf, H., Parrish, A., Petelina, S. V., Piccolo, C., Pommereau, J.-P., Randall, C. E., Robert, C., Roth, C., Schneider, M., Senten, C., Steck, T., Strandberg, A., Strawbridge, K. B., Sussmann, R., Swart, D. P. J., Tarasick, D. W., Taylor, J. R., Tétard, C., Thomason, L. W., Thompson, A. M., Tully, M. B., Urban, J., Vanhellemont, F., Vigouroux, C., von Clarmann, T., von der Gathen, P., von Savigny, C., Waters, J. W., Witte, J. C., Wolff, M., and Zawodny, J. M.: Validation of ozone measurements from the Atmospheric Chemistry Experiment (ACE), Atmos. Chem. Phys., 9, 287–343, 2009,
http://www.atmos-chem-phys.net/9/287/2009/. 2172

ESA: Envisat-GOMOS, An instrument for global atmospheric ozone monitoring, vol. SP-1244,

Title Page

Abstract | Introduction

Conclusions | References

Tables | Figures

◄◄ | ►►

◄ | ►

Back | Close

Full Screen / Esc

Printer-friendly Version

Interactive Discussion

European Space Agency, 2001. 2171

Fortuin, J. P. F. and Kelder, H.: An ozone climatology based on ozonesonde and satellite mea-surements, J. Geophys. Res., 103, 31709–31734, 1998. 2186

Harris, N., Hudson, R., and Phillips, C.: Assessment of trends in the vertical distribution of ozone, WMO, Geneva, 1999. 2175, 2182

Hassler, B., Bodeker, G. E., and Dameris, M.: Technical Note: A new global database of trace gases and aerosols from multiple sources of high vertical resolution measurements, Atmos. Chem. Phys., 8, 5403–5421, 2008, http://www.atmos-chem-phys.net/8/5403/2008/. 2186

Hauchecorne, A., Bertaux, J.-L., Dalaudier, F., Cot, C., Lebrun, J.-C., Bekki, S., Marchand, M., Kyrölä, E., Tamminen, J., Sofieva, V., Fussen, D., Vanhellemont, F., Fanton d'Andon, O., Bar-rot, G., Mangin, A., Théodore, B., Guirlet, M., Snoeij, P., Koopman, R., Saavedra de Miguel, L., Fraisse, R., and Renard, J.-B.: First simultaneous global measurements of nighttime stratospheric NO_2 and NO_3 observed by Global Ozone Monitoring by Occultation of Stars (GOMOS)/Envisat in 2003, J. Geophys. Res., 110, D18301, doi:10.1029/2004JD005711, 2005. 2171, 2172, 2185

Hood, L. L. and Soukharev, B. E.: Solar induced variations of odd nitrogen: Multiple re-gression analysis of UARS HALOE data, Geophys. Res. Lett., 33, L22805, doi:10.1029/2006GL028122, 2006. 2183

Huang, F. T., Mayr, H. G., Russell, J. M., Mlynczak, M. G., and Reber, C. A.: Ozone diurnal vari-ations and mean profiles in the mesosphere, lower thermosphere, and stratosphere, based on measurements from SABER on TIMED, J. Geophys. Res. (Space Physics), 113, A04307, doi:10.1029/2007JA012739, 2008. 2178

Jones, A., Urban, J., Murtagh, D. P., Eriksson, P., Brohede, S., Haley, C., Degenstein, D., Bourassa, A., von Savigny, C., Sonkaew, T., Rozanov, A., Bovensmann, H., and Burrows, J.: Evolution of stratospheric ozone and water vapour time series studied with satellite mea-surements, Atmos. Chem. Phys., 9, 6055–6075, 2009, http://www.atmos-chem-phys.net/9/6055/2009/. 2182

Kerzenmacher, T., Wolff, M. A., Strong, K., Dupuy, E., Walker, K. A., Amekudzi, L. K., Batchelor, R. L., Bernath, P. F., Berthet, G., Blumenstock, T., Boone, C. D., Bramstedt, K., Brogniez, C., Brohede, S., Burrows, J. P., Catoire, V., Dodion, J., Drummond, J. R., Dufour, D. G., Funke, B., Fussen, D., Goutail, F., Griffith, D. W. T., Haley, C. S., Hendrick, F., Höpfner, M., Huret, N., Jones, N., Kar, J., Kramer, I., Llewellyn, E. J., López-Puertas, M., Manney, G., McElroy, C.

Title Page

Abstract | Introduction

Conclusions | References

Tables | Figures

◄◄ | ►►

◄ | ►

Back | Close

Full Screen / Esc

Printer-friendly Version

Interactive Discussion

T., McLinden, C. A., Melo, S., Mikuteit, S., Murtagh, D., Nichitiu, F., Notholt, J., Nowlan, C., Piccolo, C., Pommereau, J.-P., Randall, C., Raspollini, P., Ridolfi, M., Richter, A., Schneider, M., Schrems, O., Silicani, M., Stiller, G. P., Taylor, J., Tétard, C., Toohey, M., Vanhellemont, F., Warneke, T., Zawodny, J. M., and Zou, J.: Validation of NO_2 and NO from the Atmospheric Chemistry Experiment (ACE), Atmos. Chem. Phys., 8, 5801–5841, 2008, http://www.atmos-chem-phys.net/8/5801/2008/. 2172

Ko, M. K. W., Sze, N.-D., and Weisenstein, D. K.: The roles of dynamical and chemical processes in determining the stratospheric concentration of ozone in one-dimensional and two-dimensional models, J. Geophys. Res., 94, 9889–9896, doi:10.1029/JD094iD07p09889, 1989. 2181

Kyrölä, E., Tamminen, J., Leppelmeier, G. W., Sofieva, V., Hassinen, S., Bertaux, J.-L., Hauchecorne, A., Dalaudier, F., Cot, C., Korablev, O., d'Andon, O. F., Barrot, G., Mangin, A., Theodore, B., Guirlet, M., Etanchaud, F., Snoeij, P., Koopman, R., Saavedra, L., Fraisse, R., Fussen, D., and Vanhellemont, F.: GOMOS on Envisat: An overview, Adv. Space Res., 33, 1020–1028, 2004. 2171

Kyrölä, E., Tamminen, J., Leppelmeier, G. W., Sofieva, V., Hassinen, S., Seppälä, A., Verronen, P. T., Bertaux, J.-L., Hauchecorne, A., Dalaudier, F., Fussen, D., Vanhellemont, F., d'Andon, O. F., Barrot, G., Mangin, A., Theodore, B., Guirlet, M., Koopman, R., Saavedra, L., Snoeij, P., and Fehr, T.: Nighttime ozone profiles in the stratosphere and mesosphere by the Global Ozone Monitoring by Occultation of Stars on Envisat, J. Geophys. Res., 111, D24306, doi: 10.1029/2006JD007193, 2006. 2171, 2173, 2186

Marsh, D. R., Garcia, R. R., Kinnison, D. E., Boville, B. A., Sassi, F., Solomon, S. C., and Matthes, K.: Modeling the whole atmosphere response to solar cycle changes in radiative and geomagnetic forcing, J. Geophys. Res. (Atmospheres), 112, D23306, doi: 10.1029/2006JD008306, 2007. 2182

McPeters, R. D., Labow, G. J., and Logan, J. A.: Ozone climatological profiles for satellite retrieval algorithms, J. Geophys. Res. (Atmospheres), 112, D05308, doi:10.1029/ 2005JD006823, 2007. 2186

Meijer, Y. J., Swart, D. P. J., Allaart, M., Andersen, S. B., Bodeker, G., Boyd, Braathena, G., Calisesia, Y., Claude, H., Dorokhov, V., von der Gathen, P., Gil, M., Godin-Beekmann, S., Goutail, F., Hansen, G., Karpetchko, A., Keckhut, P., Kelder, H. M., Koelemeijer, R., Kois, B., Koopman, R. M., Lambert, J.-C., Leblanc, T., McDermid, I. S., Pal, S., Kopp, G., Schets, H., Stubi, R., Suortti, T., Visconti, G., , and Yela, M.: Pole-to-pole validation of ENVISAT/GOMOS

Title Page

Abstract | Introduction

Conclusions | References

Tables | Figures

◄ | ►►

◄ | ►

Back | Close

Full Screen / Esc

Printer-friendly Version

Interactive Discussion

ozone profiles using data from ground-based and balloon-sonde measurements, J. Geophys. Res., 109, D23305, doi:10.1029/2004JD004834, 2004. 2172

Perliski, L. M., Solomon, S., and London, J.: On the interpretation of seasonal variations of stratospheric ozone, Planet. Space Sci., 37, 1527–1538, doi:10.1016/0032-0633(89)90143-8, 1989. 2181

Randel, W. J. and Wu, F.: A stratospheric ozone profile data set for 1979-2005: Variability, trends, and comparisons with column ozone data, J. Geophys. Res. (Atmospheres), 112, D06313, doi:10.1029/2006JD007339, 2007. 2182, 2186

Renard, J., Berthet, G., Brogniez, C., Catoire, V., Fussen, D., Goutail, F., Oelhaf, H., Pommereau, J., Roscoe, H. K., Wetzel, G., Chartier, M., Robert, C., Balois, J., Verwaerde, C., Auriol, F., François, P., Gaubicher, B., and Wursteisen, P.: Validation of GOMOS-Envisat vertical profiles of O_3, NO_2, NO_3, and aerosol extinction using balloon-borne instruments and analysis of the retrievals, J. Geophys. Res. (Space Physics), 113, A02302, doi:10.1029/2007JA012345, 2008. 2172

Seppälä, A., Verronen, P. T., Clilverd, M. A., Randall, C. E., Tamminen, J., Sofieva, V. F., Backman, L., and Kyrölä, E.: Arctic and Antarctic polar winter NO_x and energetic particle precipitation in 2002–2006, Geophys. Res. Lett., 34, L12810, doi:10.1029/2007GL029733, 2007. 2186

Smith, A. K.: Physics and chemistry of the mesopause region, J. Atmos. Sol.-Terr. Phys., 66, 839–857, 2004. 2181

Smith, A. K., Marsh, D. R., Russell, J. M., Mlynczak, M. G., Martin-Torres, F. J., and Kyrölä, E.: Satellite observations of high nighttime ozone at the equatorial mesopause, J. Geophys. Res. (Atmospheres), 113, D17312, doi:10.1029/2008JD010066, 2008. 2179

Sofieva, V. F., Kyrölä, E., Verronen, P. T., Seppälä, A., Tamminen, J., Marsh, D. R., Smith, A. K., Bertaux, J.-L., Hauchecorne, A., Dalaudier, F., Fussen, D., Vanhellemont, F., Fanton d'Andon, O., Barrot, G., Guirlet, M., Fehr, T., and Saavedra, L.: Spatio-temporal observations of the tertiary ozone maximum, Atmos. Chem. Phys., 9, 4439–4445, 2009, http://www.atmos-chem-phys.net/9/4439/2009/. 2186

Soukharev, B. E. and Hood, L. L.: Solar cycle variation of stratospheric ozone: Multiple regression analysis of long-term satellite data sets and comparisons with models, J. Geophys. Res. (Atmospheres), 111, D20314, doi:10.1029/2006JD007107, 2006. 2182

Tétard, C., Fussen, D., Bingen, C., Capouillez, N., Dekemper, E., Loodts, N., Mateshvili, N., Vanhellemont, F., Kyrölä, E., Tamminen, J., Sofieva, V., Hauchecorne, A., Dalaudier, F.,

Bertaux, J.-L., Fanton d'Andon, O., Barrot, G., Guirlet, M., Fehr, T., and Saavedra, L.: Simultaneous measurements of OClO, NO_2 and O_3 in the Arctic polar vortex by the GOMOS instrument, Atmos. Chem. Phys., 9, 7857–7866, 2009, http://www.atmos-chem-phys.net/9/7857/2009/. 2186

5 Verronen, P. T., Kyrölä, E., Tamminen, J., Funke, B., Gil-López, S., Kaufmann, M., López-Puertas, M., von Clarmann, T., Stiller, G., Grabowski, U., and Höpfner, M.: A comparison of night-time GOMOS and MIPAS ozone profiles in the stratosphere and mesosphere, Adv. Space Res., 36, 958–966, 2005. 2172

Verronen, P. T., Seppälä, A., Kyrölä, E., Tamminen, J., Pickett, H. M., and Turunen, E.: Pro-
10 duction of odd hydrogen in the mesosphere during the January 2005 solar proton event, Geophys. Res. Lett., 33, L24811, doi:10.1029/2006GL028115, 2006. 2186

Verronen, P. T., Ceccherini, S., Cortesi, U., Kyrölä, E., and Tamminen, J.: Statistical comparison of night-time NO_2 observations in 2003–2006 from GOMOS and MIPAS instruments, Adv. Space Res., 43, 1918–1925, doi:10.1016/j.asr.2009.01.027, 2009. 2172

15 WMO: Scientific Assessment of Ozone Depletion: 2006, Global Ozone Research and Monitoring Project – Report No. 50, World Meteorological Organization, Geneva, Switzerland, 2007. 2175, 2182

Title Page

Abstract | Introduction

Conclusions | References

Tables | Figures

◄ | ►

◄ | ►

Back | Close

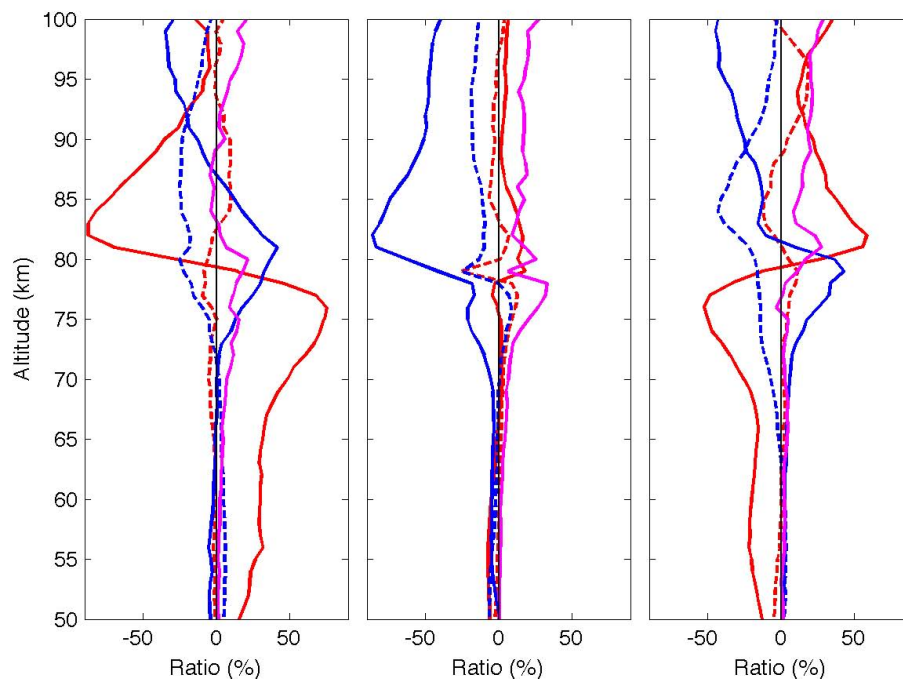Full Screen / Esc

Printer-friendly Version

Interactive Discussion
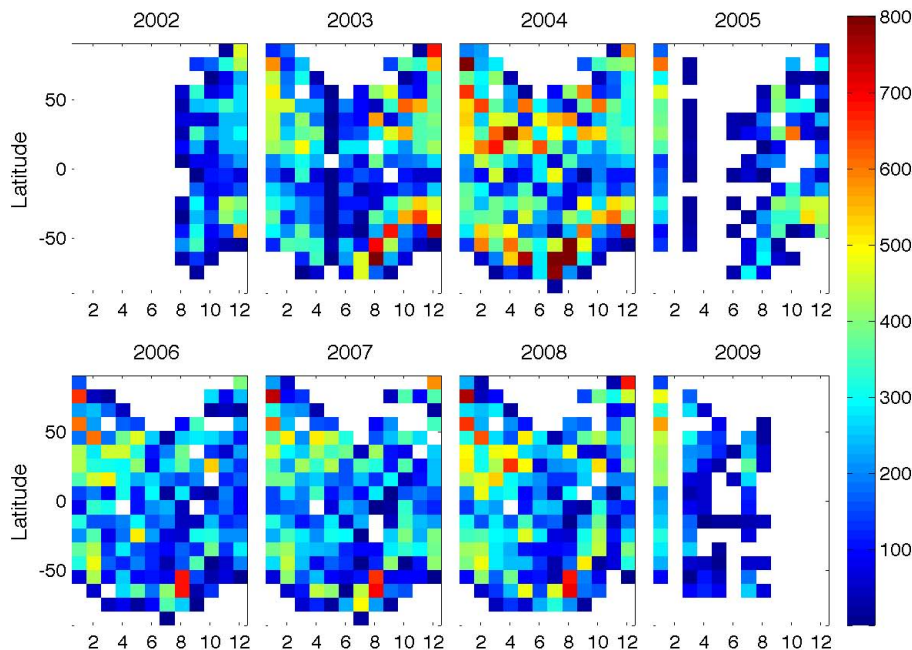
Fig. 1. Number of dark limb occultations (solar zenith angle greater than 107°) in 28 August 2002–8 August 2009 as a function of time (in months) and latitude. Measurements have been collected monthly to the 10° latitudinal grid. Occultations that have ended before the 20 km tangent height or that have the obliquity angle larger than 80° have been disregarded. The grid cells that have fewer than 2 measurements carry white colour.

ACPD

10, 2169–2220, 2010

**GOMOS trace gases
2002–2008**

E. Kyrölä
(erkki.kyrola@fmi.fi)
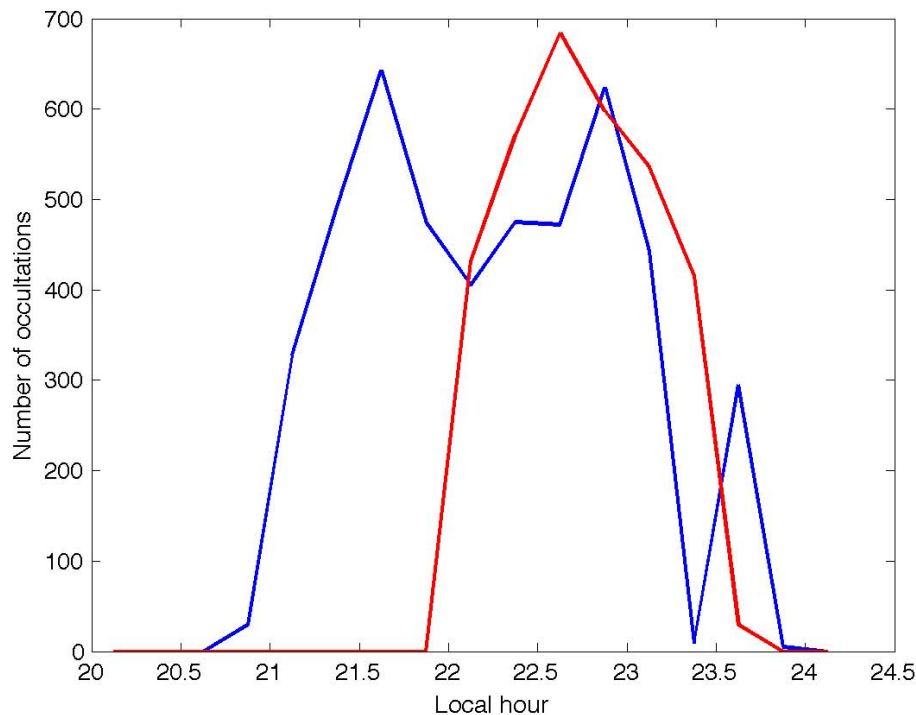
Fig. 2. The number of occultations as a function of the local time for GOMOS dark limb occultations (solar zenith angle greater than 107°) in 2004 for two latitude belts. The blue line: 5° S–5° N, the red line 40° N–50° N.

Title Page

Abstract   Introduction

Conclusions   References

Tables   Figures

◄   ►►

◄   ►

Back   Close

Full Screen / Esc

Printer-friendly Version

Interactive Discussion
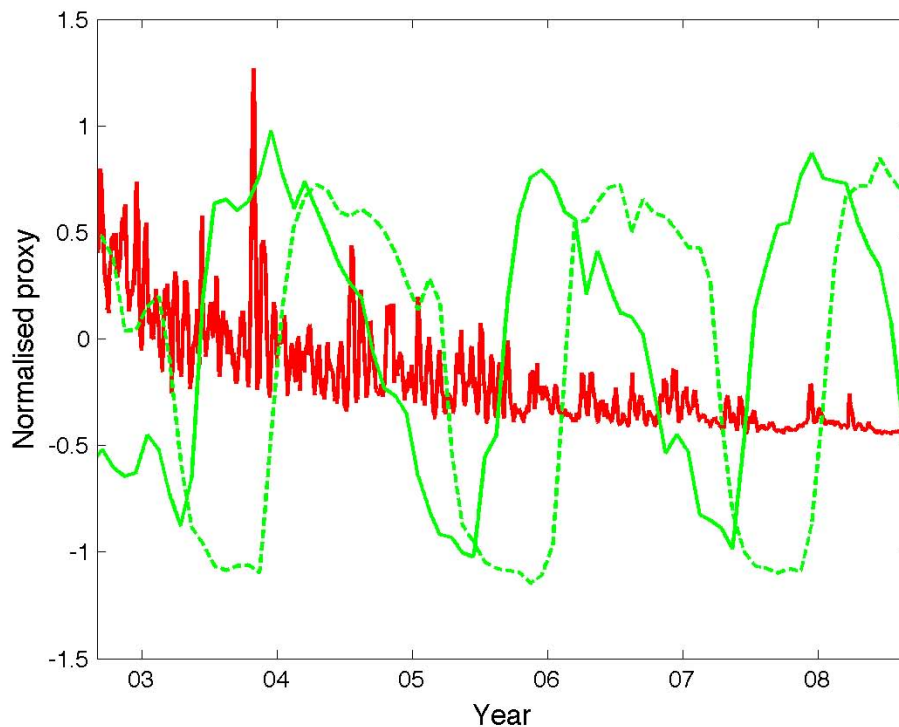
Fig. 3. The normalised proxies (see Eq. 2) as a function of time (in days). The solar F10.7 cm radio flux (red line) serves a solar proxy. The winds at 10 hPa (solid green line) and 30 hPa (dashed green line) are proxies for the QBO effects.
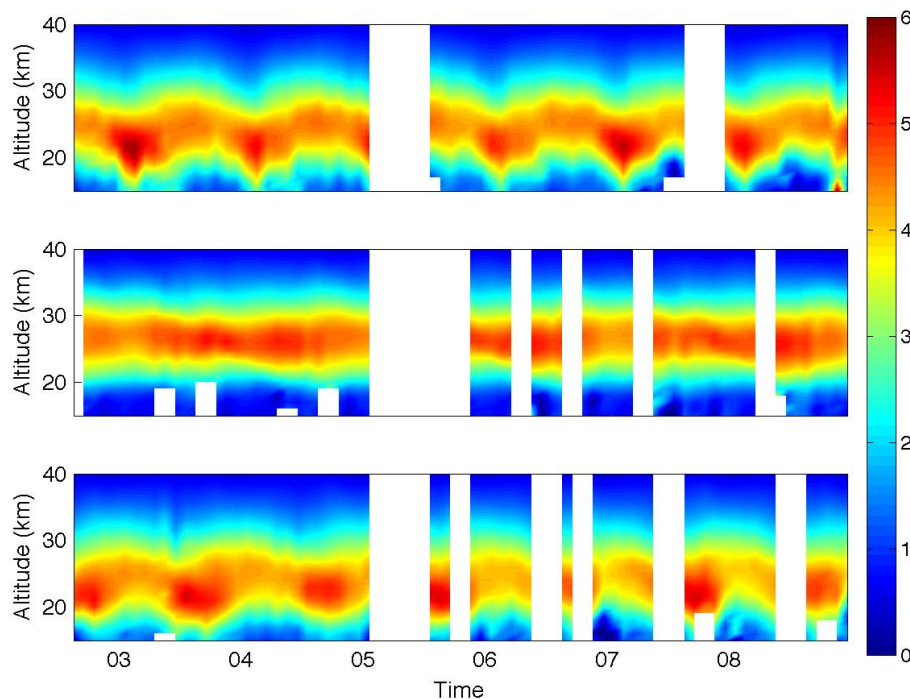
Fig. 4. Ozone number density in the stratosphere in three latitude belts as a function of time (in months) and altitude. The density is scaled by $10^{12}\,\mathrm{cm}^{-3}$. The time covered is 1 August 2002–31 December 2008. Latitude belts: 30° N–50° N (top), 10° S–10° N (middle), 30° S–50° S (bottom). White space in the panels means that there are not enough data available.
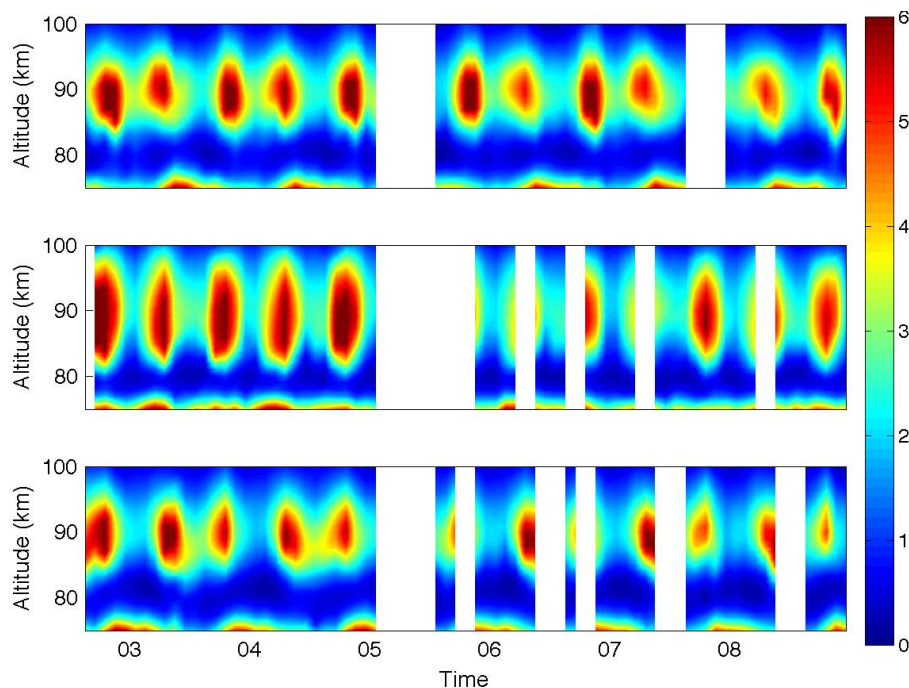
Fig. 5. Ozone number density in the MLT in three latitude belts as a function of time (in months) and altitude. The density is scaled by $10^8 \, cm^{-3}$. The time covered is 1 August 2002–31 December 2008. Latitude belts: 30° N–50° N (top), 10° S–10° N (middle), 30° S–50° S (bottom).
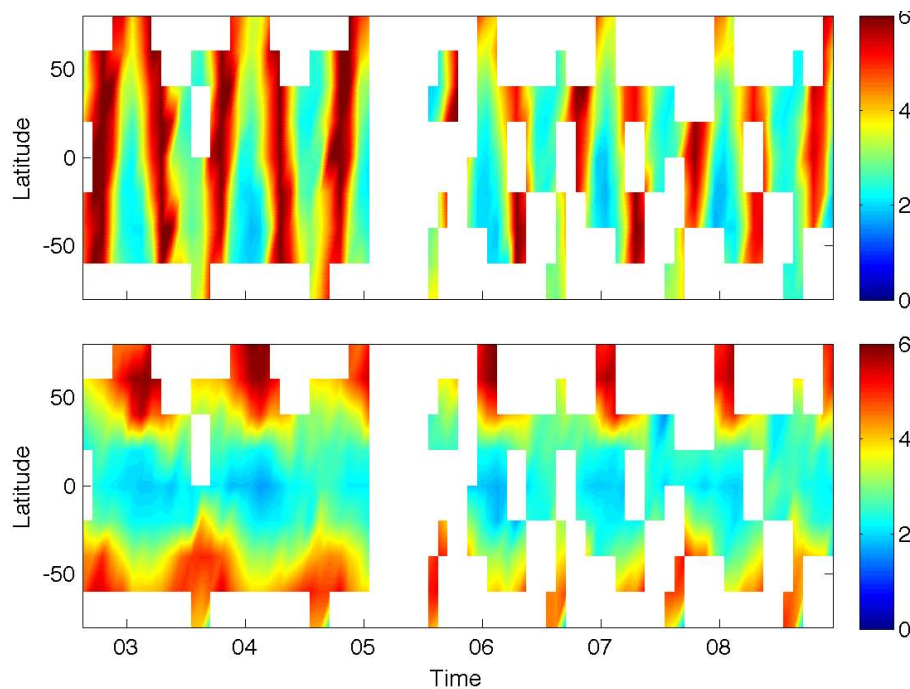
Fig. 6. Ozone number density at 90 km (upper panel, scaled by $10^8\,\mathrm{cm}^{-3}$) and 20 km (lower panel, scaled by $10^{12}\,\mathrm{cm}^{-3}$) as a function of time (in months) and latitude in 1 August 2002–31 December 2008.
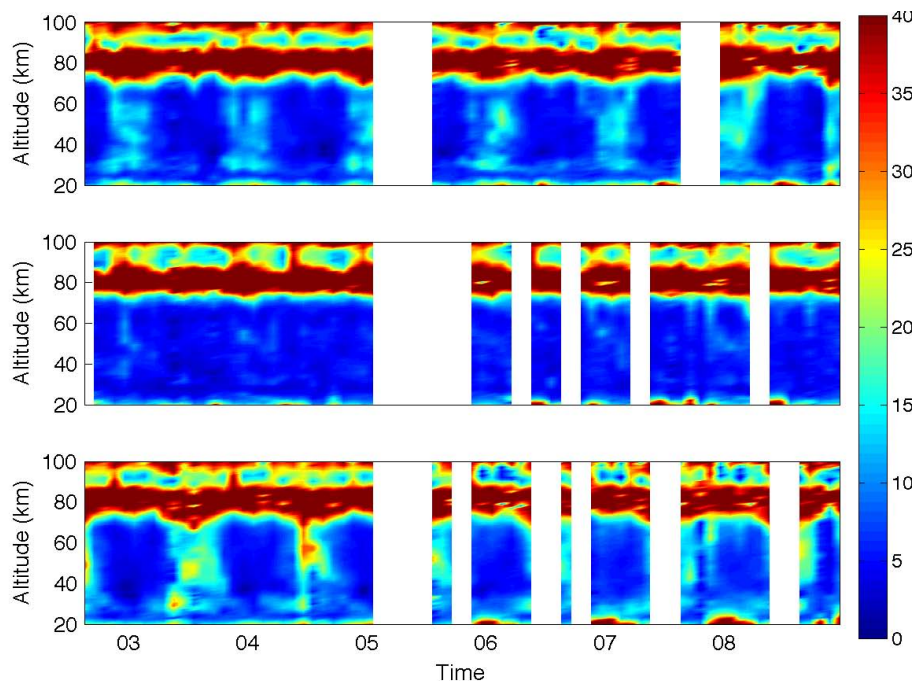
Fig. 7. Ozone variability in 15–100 km in three latitude belts as a function of time (in months) and altitude. The variability shown is the interquartile range of data subtracted by the interquartile range of the error estimates. The values are relative to median values and in %. Latitude belts: 30° N–50° N (top), 10° S–10° N (middle), 30° S–50° S (bottom).
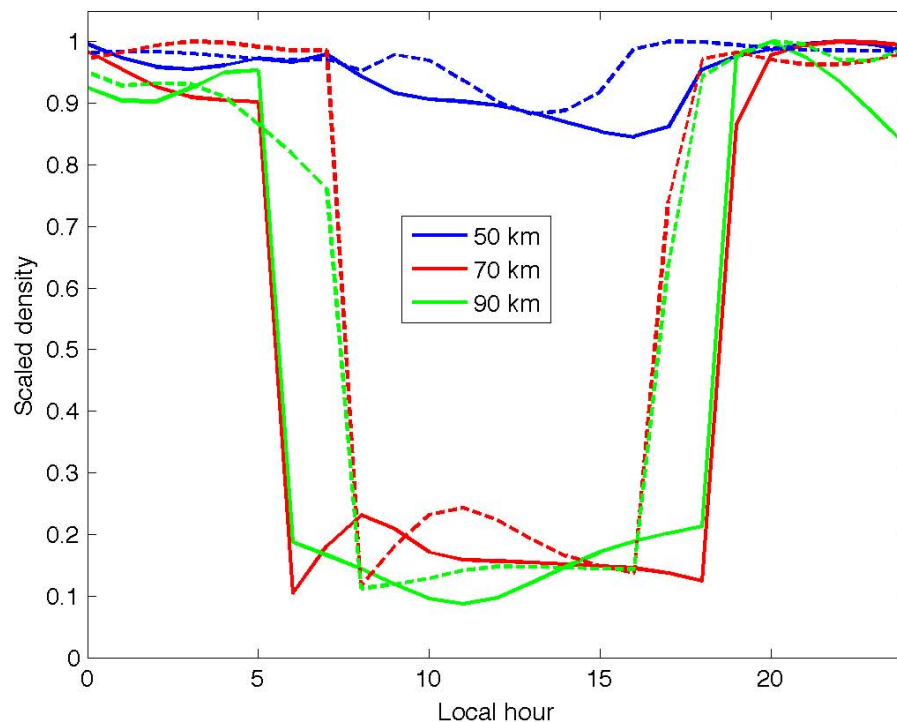
Fig. 8. Ozone number density as a function of the local time at three altitudes. Densities are calculated using the NCAR ROSE model. The solid lines are from 5° S–5° N, the dashed lines from 40° N–50° N. The number densities are scaled by the maximum values reached at a given altitude and latitude.
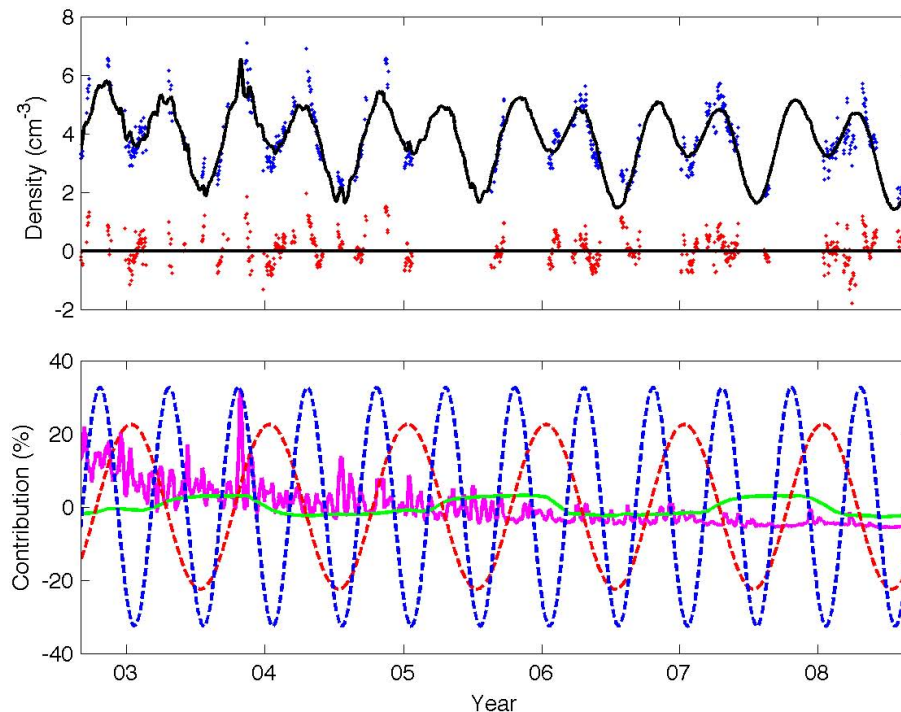
Fig. 9. An example of the O_3 number density fitting at 90 km in 40° N–50° N. Time axis unit is day. In the upper panel GOMOS measurements are shown by the blue dots and the fit by the black line. The residual is shown by red dots. All three scaled by scaled by 10^8 cm^{-3}. In the lower panel the identifications are: Annual (a_1 and b_1 contributions): dashed red, Semi-annual (a_2 and b_2 contributions): dashed blue, QBO 1 (q_1 and q_2 contributions): solid green, solar (s): solid magenta. The components have been scaled by a constant coefficient and given in %. The constant term itself has not been shown.

Full Screen / Esc

Printer-friendly Version

Interactive Discussion
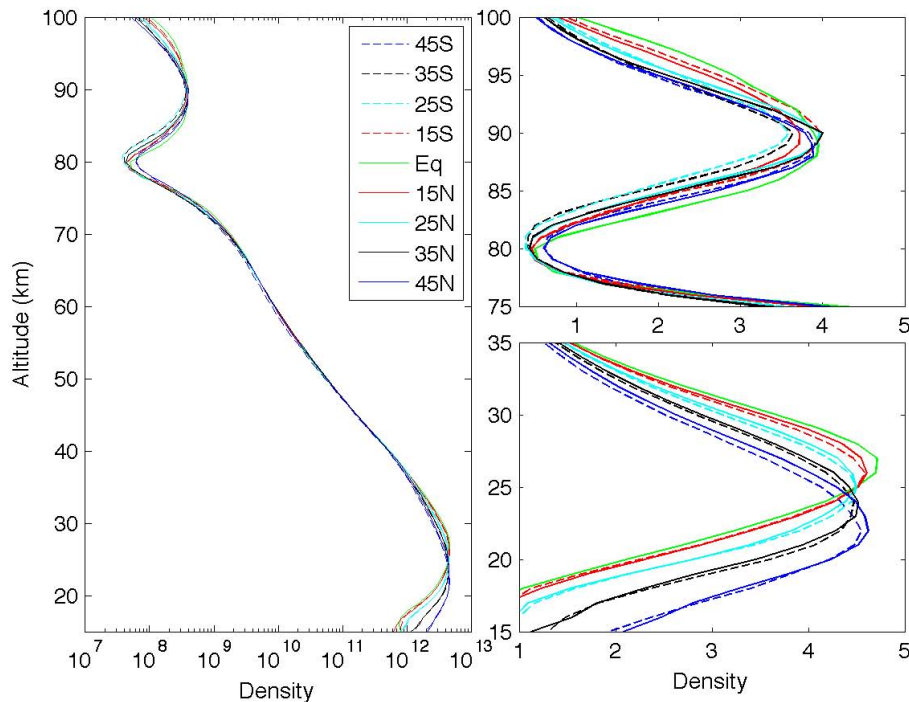
Fig. 10. The O_3 constant factor $c(z)$ as a function of altitude for several latitude belts. The panel in left shows constant profiles 15–100 km at different latitudes (unit cm^{-3}). The upper right panel shows the same profiles in the MLT (unit 10^8 cm^{-3}) and the lower right panel in the stratosphere (unit 10^{12} cm^{-3}).
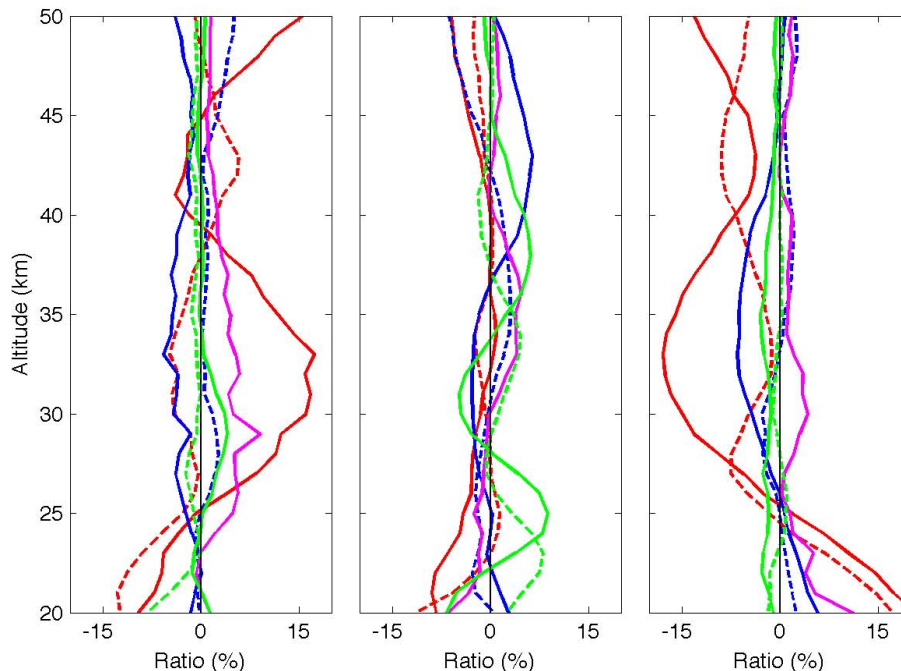
Fig. 11. The fitting components for ozone as a function of altitude in three latitude belts in the stratosphere. All amplitudes have been given as a ratio between the original amplitude in Eq. (1) and the the constant term $c(z)$ in Eq. (1) and given in %. Line identifications: annual (a_1 and b_1): solid and dashed red, respectively, Semi-annual (a_2 and b_2): solid and dashed blue, respectively, QBO 10 hPa (q_1) and 30 hPa (q_2): solid and dashed green, respectively, solar (s): solid magenta. The zero value line has been shown by a thin black line. Left: 50° S–40° S, Middle: 10° S–10° N, Right: 40° N–50° N.

Fig. 12. The fitting components as a function of altitude in three latitude belts in the MLT. All amplitudes have been given as a ratio between the original amplitude in Eq. (1) and the the constant term $c(z)$ in Eq. (1) and given in %. Line identifications: Annual (a_1 and b_1): solid and dashed red, respectively. Semi-annual (a_2 and b_2): solid and dashed blue, respectively, solar (s): solid magenta. The QBO values are not shown. The zero value line has been shown by a thin black line. Left: 50° S–40° S, Middle: 10° S–10° N, Right: 40° N–50° N.
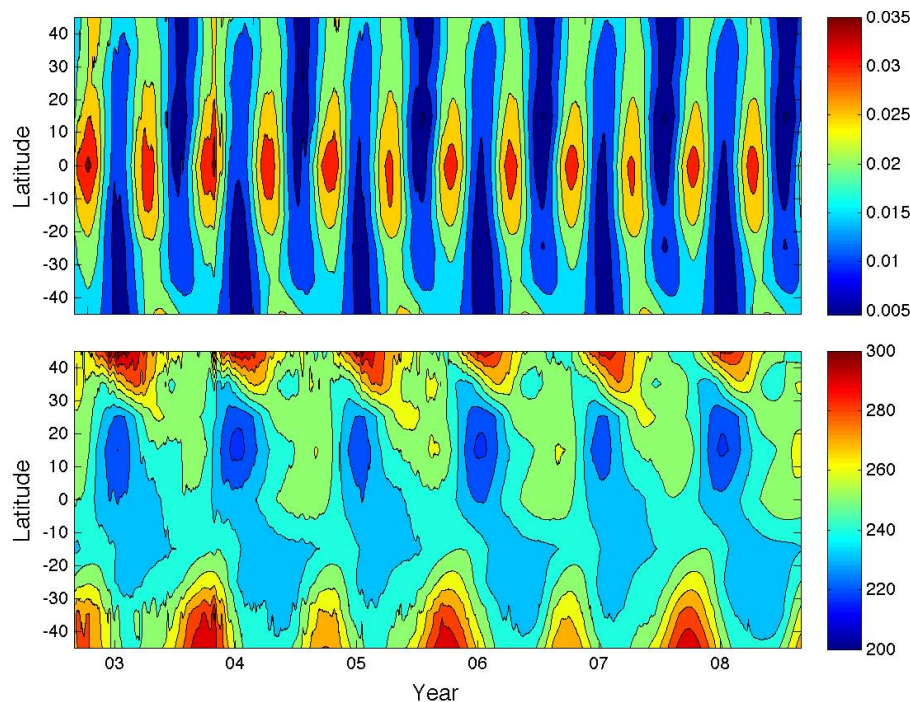
Fig. 13. The vertical partial ozone columns as a function of time (in days) and latitude. The columns are calculated from the time series. The upper panel gives the partial column in 80–100 km and the lower panel the partial column in 15–100 km. The unit in both figures is Dobson (2.69×10^{16} molecules cm^{-2}).
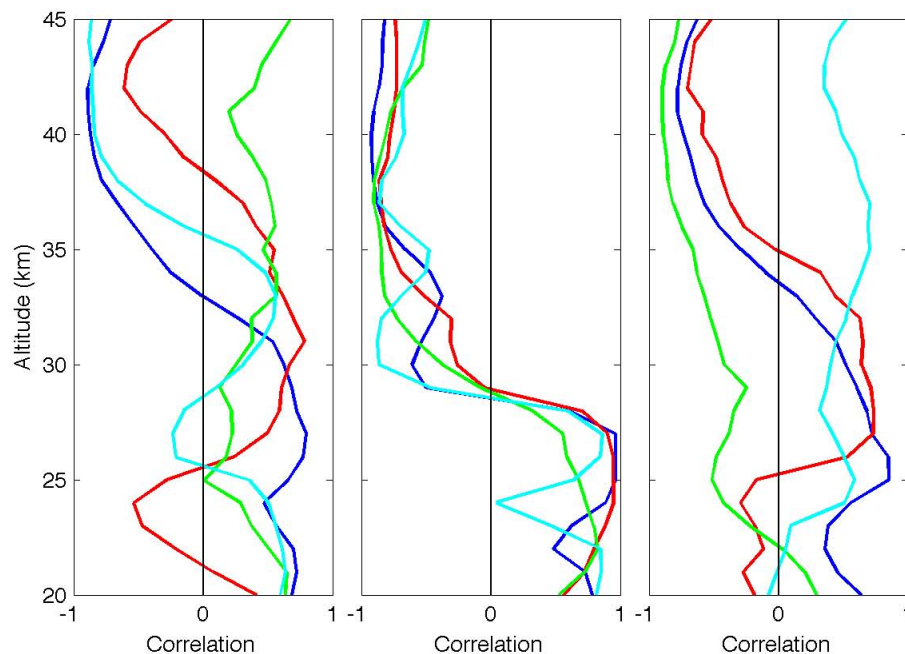
Fig. 14. Correlations of monthly GOMOS ozone median densities with the monthly median temperatures (from ECMWF) as a function of altitude. Left: 30° S–50° S, Middle: 10° S–10° N, Right: 30° N–50° N. Line identifications: DJF: blue, MAM: red, JJA: green, SON: cyan.
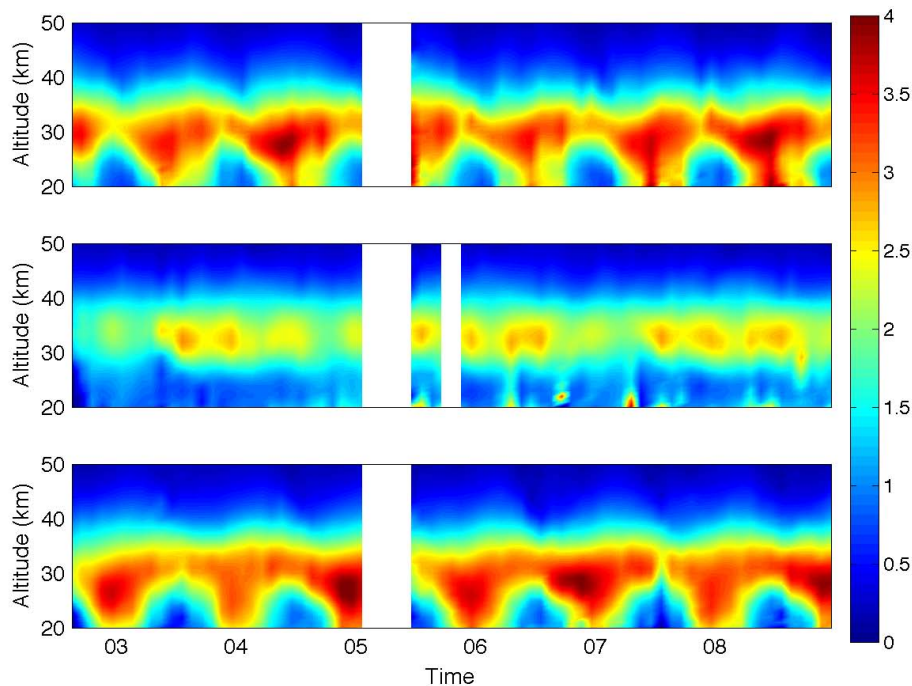
Fig. 15. NO_2 number density in stratosphere in three latitude belts in 2002–2008 as a function of time (in months) and altitude. The density is scaled by $10^9 \, cm^{-3}$. The time covered is 1 August 2002–31 December 2008. Latitude belts: 30° N–50° N (top), 10° S–10° N (middle), 30° S–50° S (bottom).
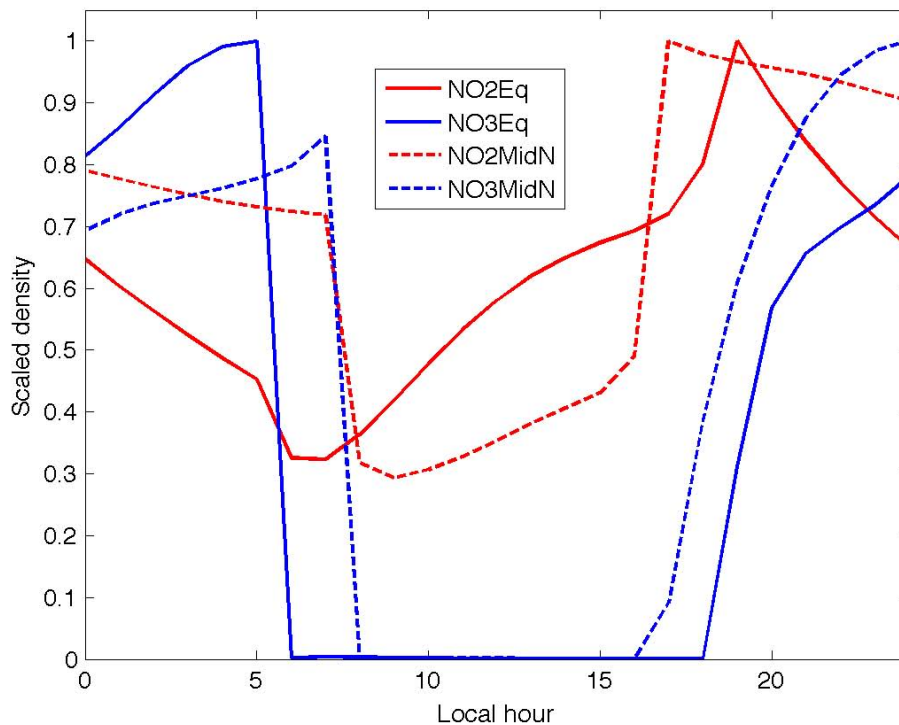
Fig. 16. NO_2 number density vs. local time at 30 km and NO_3 number density vs local time at 40 km. The number densities are scaled by the maximum values reached at a given altitude and latitude. Results are from the NCAR ROSE model. The solid lines are for the equator and dashed lines for mid-latitudes.
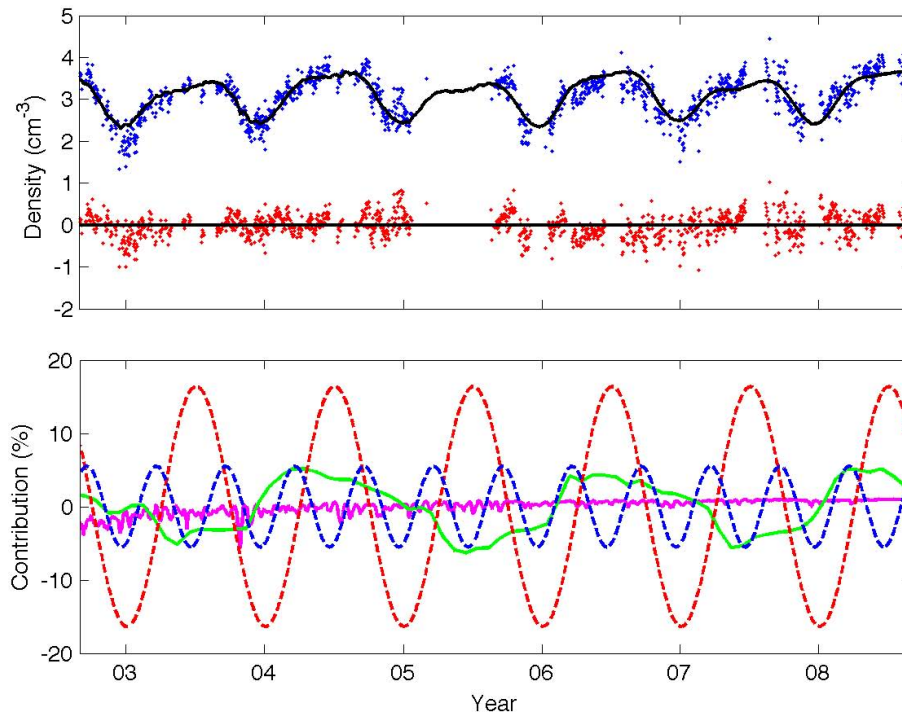
Fig. 17. Example of the NO$_2$ number density fitting at 30 km in the 40° N–50° N latitude band. Time axis unit is day. In the upper panel GOMOS measurements are shown by the blue dots and the fit by the black line. The residual is shown by red dots. All three scaled by scaled by 10^9 cm^{-3}. In the lower panel the identifications are: annual (a_1 and b_1 contributions): dashed red, Semi-annual (a_2 and b_2 contributions): dashed blue, QBO 1 (q_1 and q_2 contributions): solid green, solar (s): solid magenta. The components have been scaled by a constant coefficient and given in %. The constant term itself has not been shown.
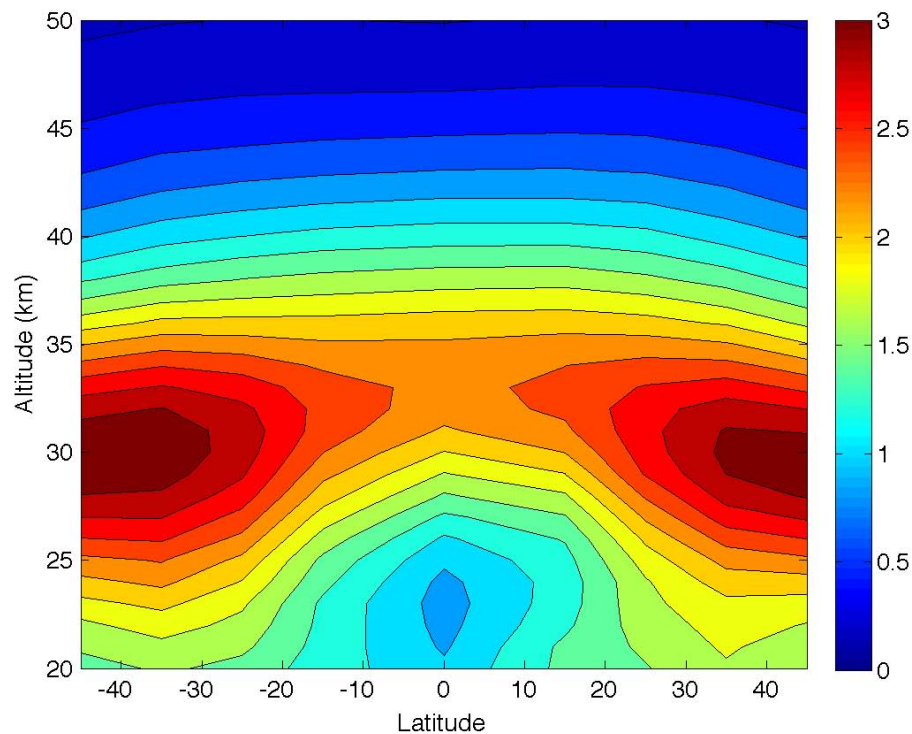
Fig. 18. The constant factor $c(z)$ in the NO_2 time series as a function of latitude and altitude. The scale is $10^9 \, cm^{-3}$.
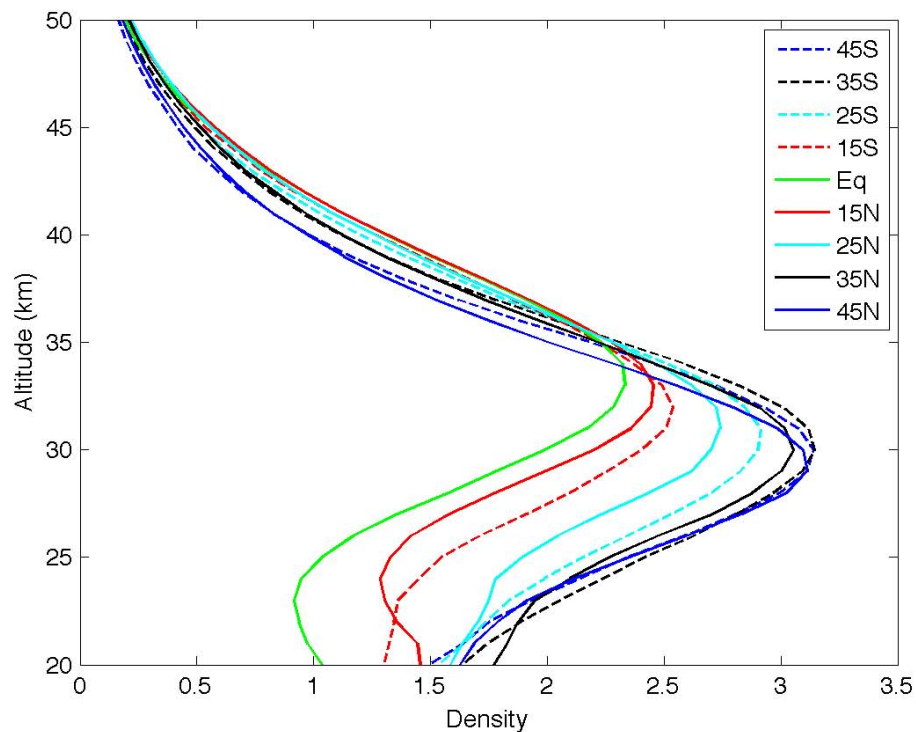
Fig. 19. The NO_2 constant factor profiles $c(z)$ as a function of altitude for several latitude belts. The scale is $10^9 \, cm^{-3}$.
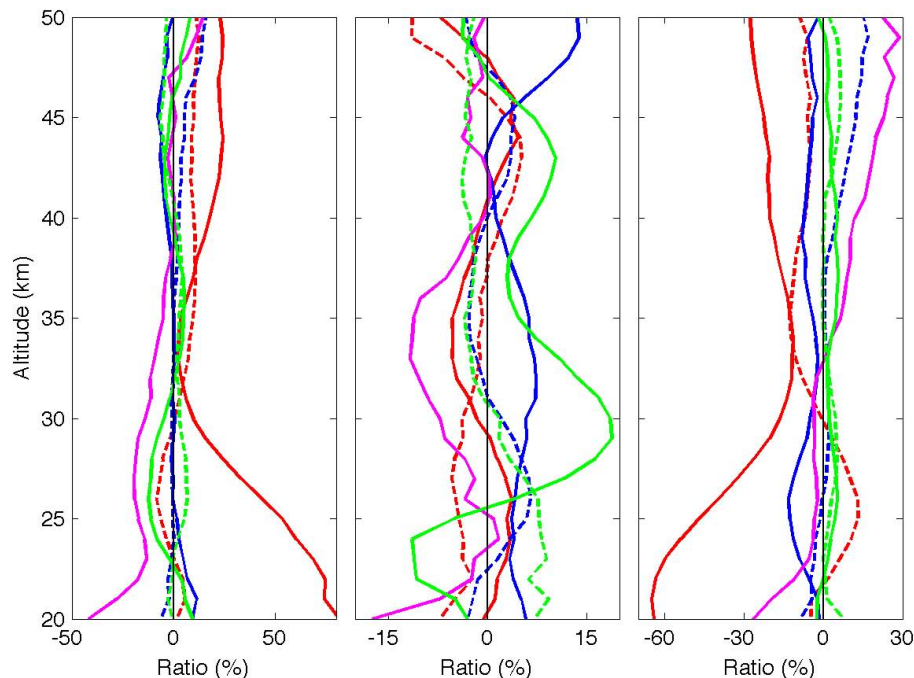
Fig. 20. The NO$_2$ fitting components as a function of altitude in three latitude belts in the stratosphere. All amplitudes have been given as a ratio between the original amplitude in Eq. (1) and the the constant term $c(z)$ in Eq. (1) and given in %. Line identifications: Annual (a_1 and b_1): solid and dashed red, respectively, Semi-annual (a_2 and b_2): solid and dashed blue, respectively, QBO 10 hPa (q_1) and 30 hPa (q_2): solid and dashed green, respectively, solar (s): solid magenta. The zero value line has been shown by a thin black line. Left: 50° S–40° S, Middle: 10° S–10° N, Right: 40° N–50° N. Note that the x-axis ranges vary in panels.

Fig. 21. The vertical partial NO_2 column in 20–50 km as a function of time (in days) and latitude. The column is calculated from the time series and scaled by 10^{15} molecules cm^{-2}.
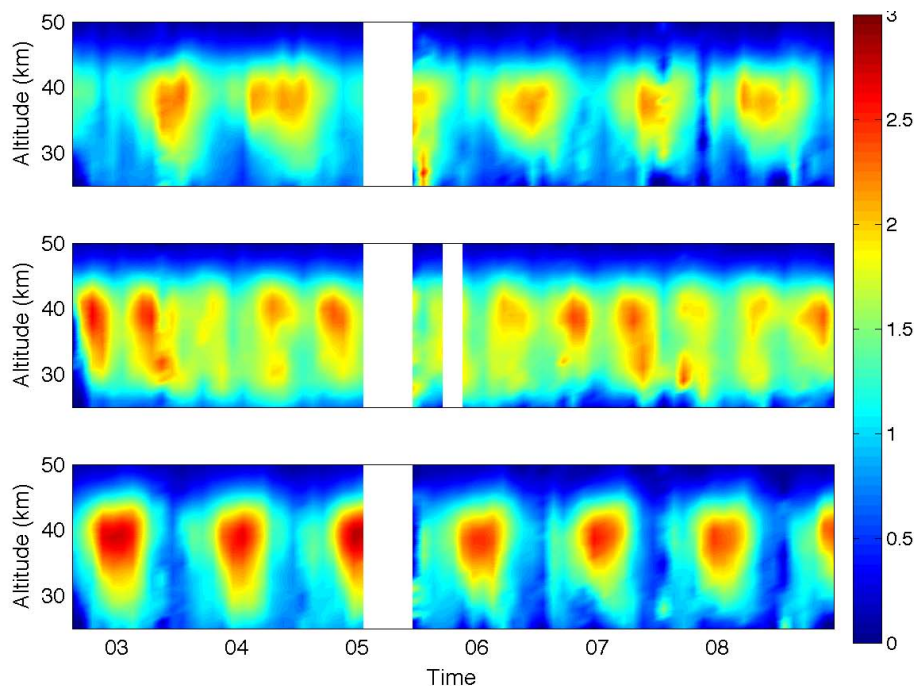
Fig. 22. NO$_3$ number density in stratosphere in three latitude belts in 2002–2008 as a function of time (in months) and altitude. The density is scaled by $10^7\,cm^{-3}$. The time covered is 1 August 2002–31 December 2008. Latitude belts: 30° N–50° N (top), 10° S–10° N (middle), 30° S–50° S (bottom).

Title Page

Abstract | Introduction

Conclusions | References

Tables | Figures

◄◄ | ►►

◄ | ►

Back | Close

Full Screen / Esc

Printer-friendly Version

Interactive Discussion
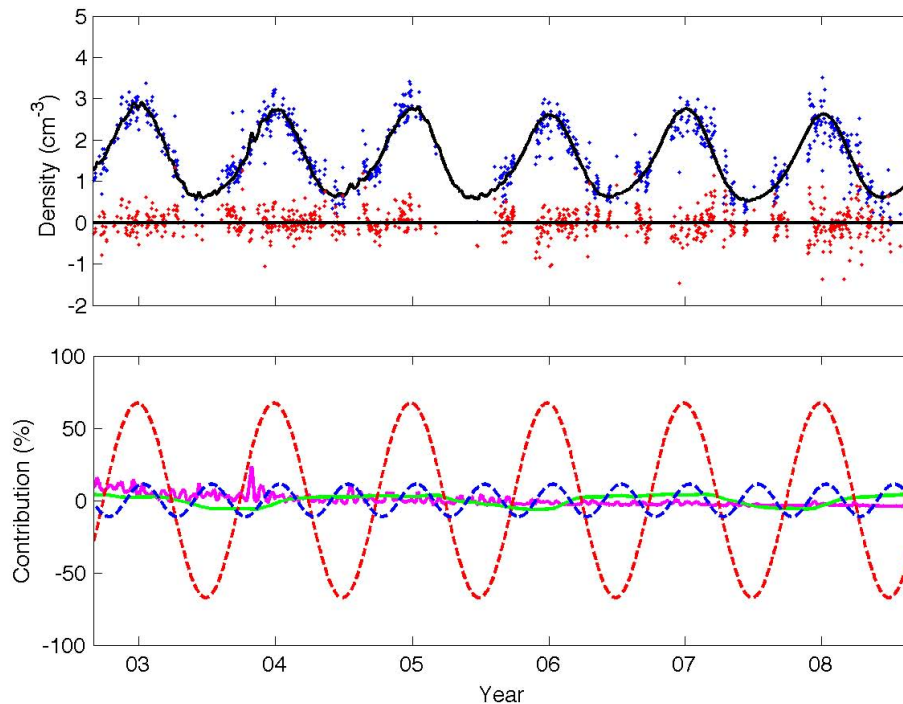
Fig. 23. Example of the NO$_3$ number density fitting at 40 km in 40° S–50° S. Time axis unit is day. In the upper panel GOMOS measurements are shown by the blue dots and the fit by the black line. The residual is shown by red dots. All three scaled by scaled by 10^7 cm^{-3}. In the lower panel the identifications are: Annual (a_1 and b_1 contributions): dashed red, Semi-annual (a_2 and b_2 contributions): dashed blue, QBO 1 (q_1 and q_2 contributions): solid green, solar (s): solid magenta. The components have been scaled by a constant coefficient and given in %. The constant term itself has not been shown.
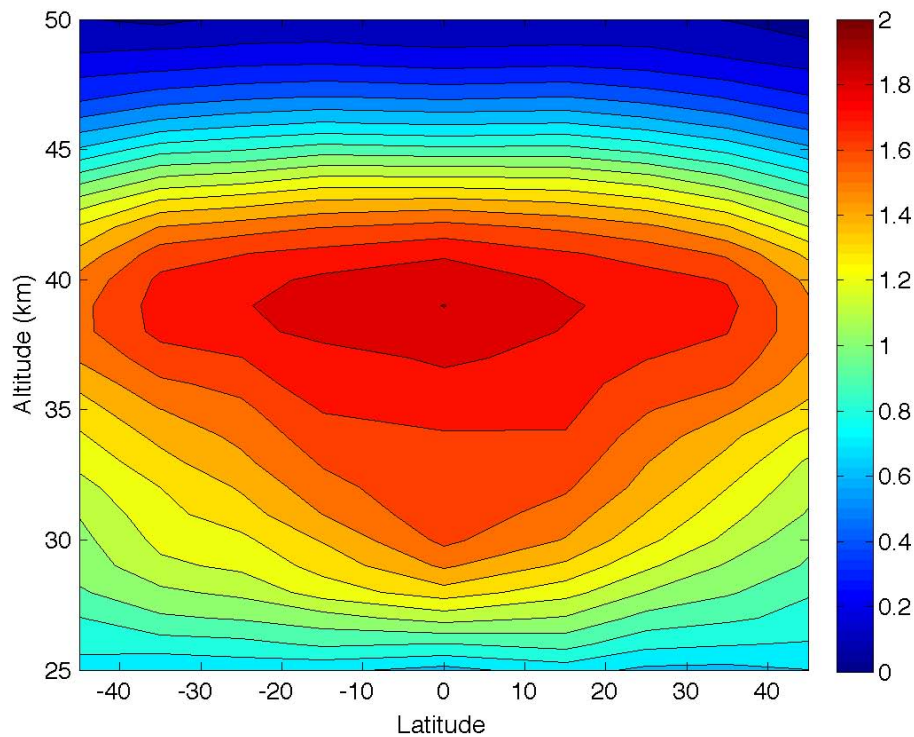
Fig. 24. NO_3 constant term $c(z)$ from the time series as a function of latitude and altitude. The scale is 10^7 cm^{-3}.

Printer-friendly Version

Interactive Discussion
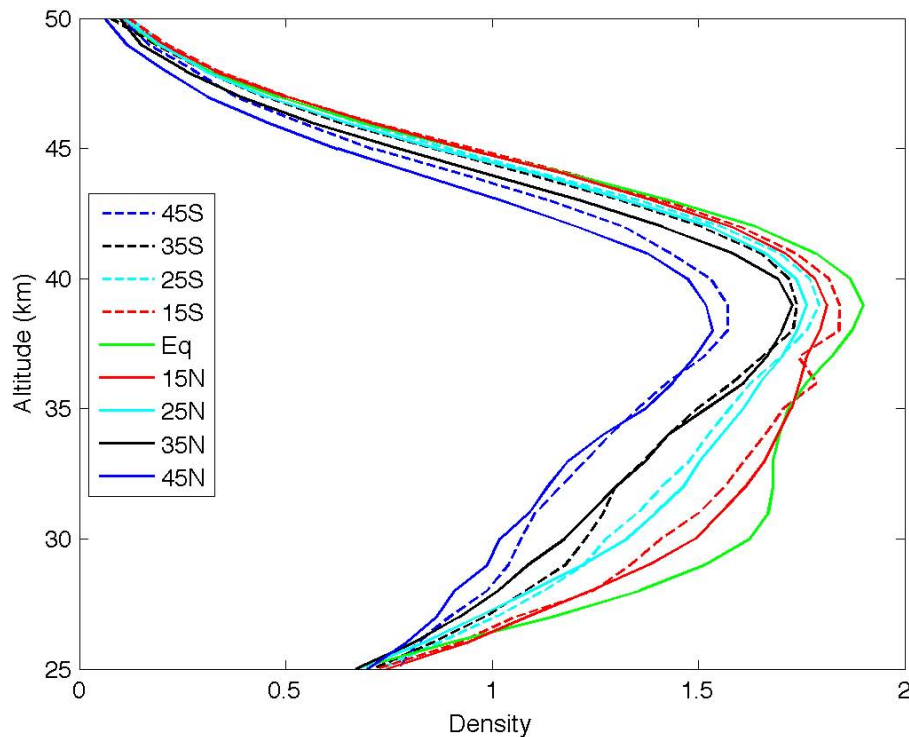
Fig. 25. The NO_3 constant factor $c(z)$ as a function of altitude for several latitude belts. Profiles are scaled by $10^7 \, cm^{-3}$.
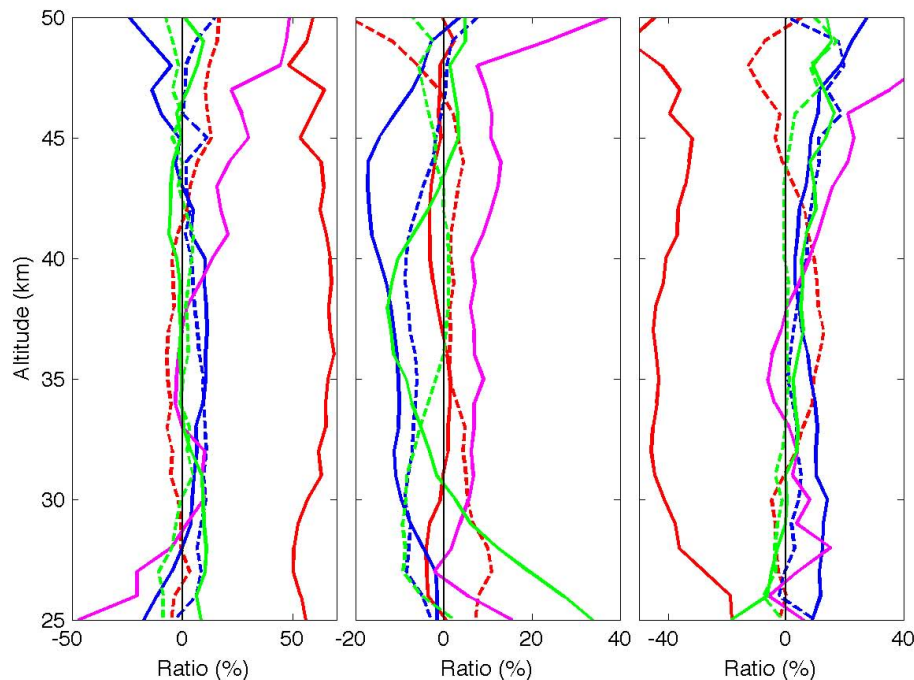
Fig. 26. The NO_3 fitting components as a function of altitude in three latitude belts in the stratosphere. All amplitudes have been given as a ratio between the original amplitude in Eq. (1) and the the constant term $c(z)$ in Eq. (1) and given in %. Line identifications: Annual (a_1 and b_1): solid and dashed red, respectively, Semi-annual (a_2 and b_2): solid and dashed blue, respectively, QBO 10 hPa (q_1) and 30 hPa (q_2): solid and dashed green, respectively, solar (s): solid magenta. The zero value line has been shown by a thin black line. Left: 50°S–40°S, Middle: 10°S–10°N, Right: 40°N–50°N. Note that the x-axis ranges vary in panels.
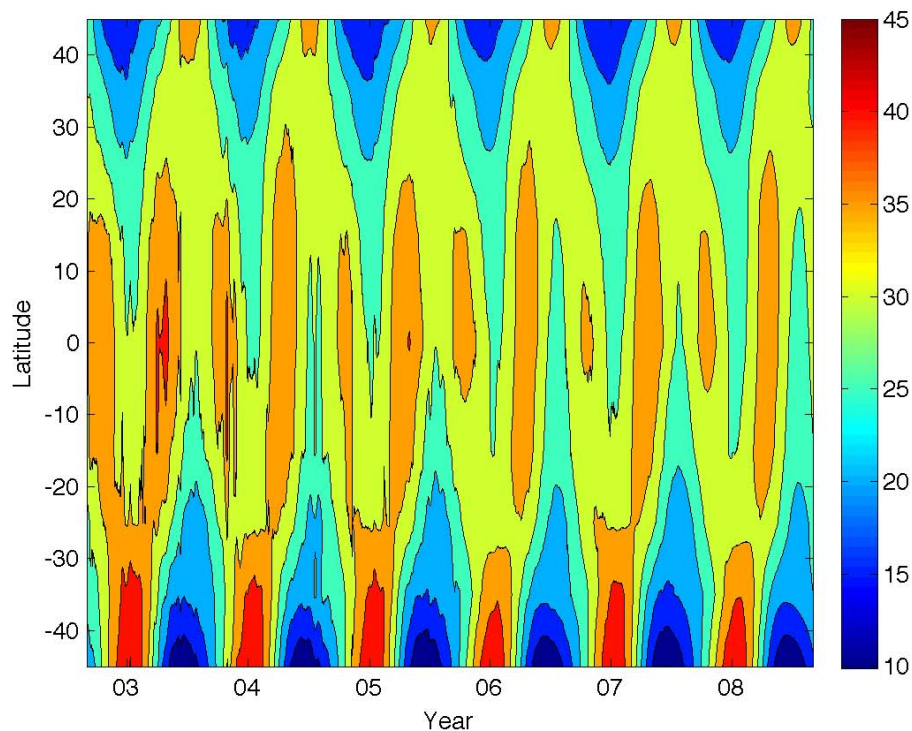
Fig. 27. The vertical partial NO_3 column in 25–50 km as a function of time (in days) and latitude The column is calculated from the time series and scaled by 10^{12} molecules cm^{-2}.
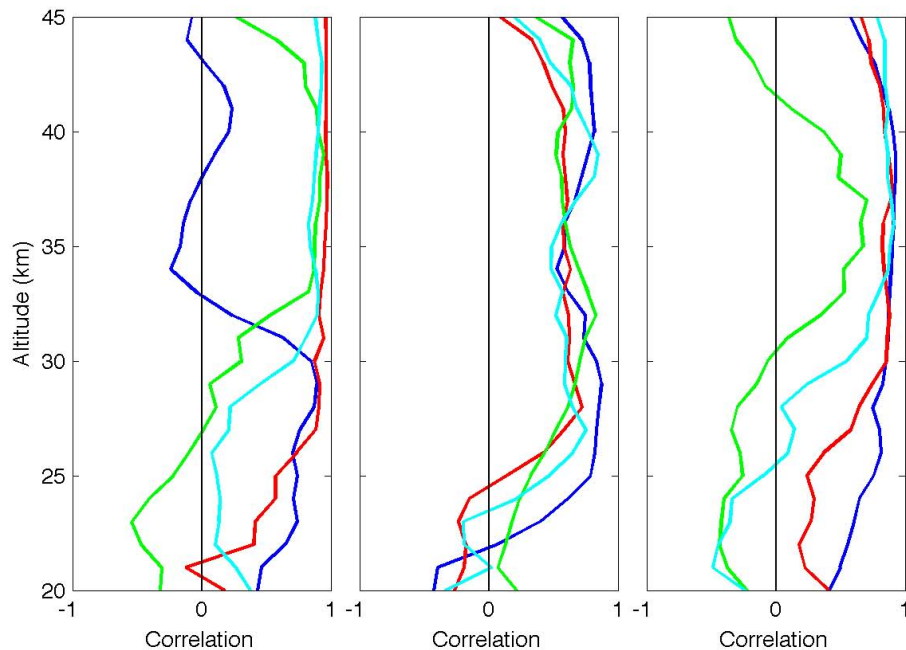
Fig. 28. Correlations of monthly GOMOS NO_3 median densities with the monthly median temperatures (from ECMWF) as a function of altitude.. Left: 30° S–50° S, Middle: 10° S–10° N, Right: 30° N–50° N. Line identifications: DJF: blue, MAM: red, JJA: green, SON: cyan.